

PERFORMANCE OF CONCRETE GRAVITY DAMS UNDER EARTHQUAKE  
EFFECTS

A THESIS SUBMITTED TO  
THE GRADUATE SCHOOL OF NATURAL AND APPLIED SCIENCES  
OF  
MIDDLE EAST TECHNICAL UNIVERSITY

BY

BERAT FEYZA SOYSAL

IN PARTIAL FULFILLMENT OF THE REQUIREMENTS  
FOR  
THE DEGREE OF MASTER OF SCIENCE  
IN  
CIVIL ENGINEERING

JANUARY 2014



Approval of the thesis:

**PERFORMANCE OF CONCRETE GRAVITY DAMS UNDER  
EARTHQUAKE EFFECTS**

submitted by **BERAT FEYZA SOYSAL** in partial fulfillment of the requirements  
for the degree of **Master of Science in Civil Engineering Department, Middle  
East Technical University** by,

Prof. Dr. Canan Özgen  
Dean, Graduate School of **Natural and Applied Sciences**

\_\_\_\_\_

Prof. Dr. Ahmet Cevdet Yalçın  
Head of Department, **Civil Engineering**

\_\_\_\_\_

Assoc. Prof. Dr. Yalın Arıcı  
Supervisor, **Civil Engineering Dept., METU**

\_\_\_\_\_

**Examining Committee Members:**

Prof. Dr. Mehmet Utku  
Civil Engineering Dept., METU

\_\_\_\_\_

Assoc. Prof. Dr. Yalın Arıcı  
Civil Engineering Dept., METU

\_\_\_\_\_

Prof. Dr. Barış Binici  
Civil Engineering Dept., METU

\_\_\_\_\_

Assoc. Prof. Dr. Afşin Sarıtaş  
Civil Engineering Dept., METU

\_\_\_\_\_

M.Sc Altuğ Akman  
ES Project Engineering and Consultancy

\_\_\_\_\_

**DATE:** 29.01.2014

**I hereby declare that all information in this document has been obtained and presented in accordance with academic rules and ethical conduct. I also declare that, as required by these rules and conduct, I have fully cited and referenced all material and results that are not original to this work.**

Name, Last name : BERAT FEYZA SOYSAL

Signature :

## **ABSTRACT**

### **PERFORMANCE OF CONCRETE GRAVITY DAMS UNDER EARTHQUAKE EFFECTS**

Soysal, Berat Feyza

M.Sc., Department of Civil Engineering

Supervisor: Assoc. Prof. Dr. Yalın Arıcı

January 2014, 83 pages

Concerns about the seismic safety of gravity dams have increased with the construction of numerous new dams in the developing world as well as the need for the evaluation of existing dam stock in the developed countries. The common procedure for the design of concrete gravity dams has been linear analyses: there is scant experience on the design of such systems using nonlinear analyses as the post-linear behavior and performance limits of gravity dam monoliths are not well known. This study is focused on the investigation of the behavior of a concrete gravity dam monolith using the incremental dynamic analysis (IDA) procedure with the goal of determining the development of damage on the monolith and the corresponding cracking patterns. The constitutive model used was first calibrated to experimental data in order to verify the ability of the model to simulate the fracture in this material. IDA was then conducted using 21 different ground motions in order to assess the state of damage on the monolith for increasing intensity measures (IM). The results show that in lieu of spectral acceleration, velocity based IMs are more effective in determining the damage process on the monolith. A simple equation for the prediction of the damage development was proposed based on the velocity characteristics of the ground motion. Finally, the results of the IDA were compared

to the static pushover analysis results in order to evaluate the scope of possible use of such analyses for determining the performance levels of dams.

**Keywords:** Concrete Gravity Dam, Smeared Crack Model, Nonlinear Analysis, Incremental Dynamic Analysis, Static Pushover Analysis.

## ÖZ

### BETON AĞIRLIK BARAJLARIN DEPREM YÜKLERİ ALTINDA PERFORMANSI

Soysal, Berat Feyza

Yüksek Lisans, İnşaat Mühendisliği Bölümü

Tez Yöneticisi: Doç. Dr. Yalın Arıcı

Ocak 2014, 83 sayfa

Gelişmekte olan ülkelerde inşa edilen birçok baraj yanında, gelişmiş ülkelerin de baraj stoklarının güvenliğinin kontrol edilmesi gerekliliği beton barajların sismik güvenilirliği hakkında çalışmaları arttırmaktadır. Beton ağırlık barajlarının tasarımında genelde doğrusal analizler kullanılmaktadır. Doğrusal olmayan analizlerle bu tip yapıların analizinde tecrübe çok sınırlıdır: zira bu yapıların doğrusal olmayan durumda davranışı ve performans limitleri hakkında gözlem ve bilgi oldukça azdır. Bu çalışmada beton ağırlık baraj davranışı monolitte oluşan hasarın gelişimi ve buna bağlı çatlama düzenlerinin elde edilmesi amacı ile artımlı dinamik analiz yöntemi ile incelenmiştir. Öncelikle malzeme modeli literatürden elde edilen deney sonuçları ile karşılaştırılarak kullanılan çatlak modelinin performansı gerçekleştirilmiştir. Bir sonraki adımda 21 değişik deprem kaydı kullanılarak yapılan artımlı dinamik analizlerle barajdaki hasarın gelişimi ve deprem kayıtlarının çeşitli şiddet ölçümleri arasındaki ilişki incelenmiştir. Baraj monolitindeki hasarı belirlemede spektral ivme değeri yerine hız ile ilgili şiddet değerlerinin daha başarılı olduğu görülmüştür. Monolitteki hasarı öngörmek için deprem kayıtlarının hız karakterlerine dayanan basit bir denklem önerilmiştir. Son olarak, statik itme

analizlerinin monolit performansını belirlemek için kullanılma olanađını incelemek üzere artımlı dinamik analiz sonuçları ile statik analiz sonuçları karşılaştırılmıřtır.

**Anahtar Kelimeler:** Beton Ađırlık Baraj, Yayılı atlak Modeli, Doğrusal Olmayan Analiz, Artımlı Dinamik Analiz, Statik İtme Analizi.

*To my parents...*

## ACKNOWLEDGEMENTS

Above all others, I would like to express my gratitude to my supervisor Assoc. Prof. Dr. Yalın Arıcı for his guidance, advice, criticism, encouragement and insight throughout the research. He has been a brilliant supervisor and mentor. It was an honor to work with him.

Prof. Dr. Barış Binici is also sincerely acknowledged for his valuable support.

I would like to thank my co-workers Alper Aldemir and Okan Koçkaya for their help whenever I needed.

I would like to express my gratitude to my friends Elif Gökçe Öz, Ezgi Berberoğlu-Yılmaz, Melis Aysun Ekici, Arzu İpek Yılmaz, Can Özbay, Görkem Deniz Köksoy and Deniz Yılmaz-Karaeren. Finally, I would like to express special thanks to Utku Albostan, for being there for me with his continuous support.

I express my sincere appreciation to my dear family for their understanding and their endless support: my mother Zehra Soysal, my father Fatih Soysal and my brother and his wife Furkan-Simten Soysal.

This study has been conducted with the funding provided by The Scientific and Technological Research Council of Turkey (TUBITAK) under the grant MAG111M712.

## TABLE OF CONTENTS

ABSTRACT.....	v
ÖZ.....	vii
ACKNOWLEDGEMENTS.....	x
TABLE OF CONTENTS.....	xi
LIST OF FIGURES.....	xiii
LIST OF TABLES.....	xv
CHAPTERS	
1. INTRODUCTION.....	1
1.1 General.....	1
1.2 Literature Review .....	2
1.3 Concrete Constitutive Modeling.....	6
1.3.1 Multi-Directional Fixed Crack Model .....	8
1.3.2 Total Strain Crack Model.....	9
1.3.3 Post-Peak Response .....	9
1.4 Finite Element Model and the Element Library .....	10
1.4.1 Q8AXI Element.....	10
1.4.2 CT12M Element .....	11
1.4.3 L6BEN Element .....	12
1.4.4 CQ16M Element.....	12
1.5 Objectives and Scope.....	13
2. CALIBRATION TESTS.....	15
2.1 Introduction .....	15
2.2 Analytical Simulation of Direct Tension Tests .....	16
2.2.1 Investigation of the Effect of Mesh Density .....	18
2.3 Analytical Simulation of a Notched Model Concrete Dam .....	20
2.3.1 Investigation of CMOD Displacement .....	21
2.3.2 Investigation of Cracking Pattern.....	25

2.4	Pseudo-Dynamic Earthquake Simulation and Analytical Pushover Analysis.....	27
2.4.1	Static Earthquake Simulation.....	29
2.4.2	Analytical Simulation of the Pushover Experiment.....	31
2.5	Analytical Simulation of Shake Table Testing on a Scaled Gravity Dam ..	32
2.5.1	Shake Table Test and Specimen .....	32
2.5.2	Analysis Results.....	34
2.5.3	Investigation of the Effect of Modeling Parameters on the Crack Location and Propagation .....	37
2.5.3.1	The Effect of Tension Softening Functions and Fracture Energy	38
2.5.3.2	The Effect of Mesh Density.....	40
2.5.4	The Effect of the Time Stepping Factor .....	43
2.5.5	Detailed Investigation of the Simulation of Crack Opening .....	45
2.5.5.1	The Effect of the Material Modeling.....	45
2.5.5.2	The Effect of the Shear Retention Factor .....	46
2.5.5.3	The Effect of Rayleigh Damping .....	48
2.5.5.4	Second Cracking Test.....	49
2.6	Summary.....	50
3.	INCREMENTAL DYNAMIC ANALYSIS OF A CONCRETE GRAVITY DAM.....	53
3.1	Introduction.....	53
3.2	Gravity Dam Model.....	53
3.2.1	Incremental Dynamic Analysis .....	56
3.3	Selection of Ground Motions.....	57
3.4	Results of IDA .....	59
3.5	Pushover Analysis .....	69
4.	CONCLUSION AND FUTURE PLANS.....	75
4.1	Conclusion .....	75
4.2	Future Plans .....	77
	REFERENCES.....	79

## LIST OF FIGURES

### FIGURES

Figure 1-1 A Schematic Drawing for the Dam Cross-Sections, (the dotted lines show the cracking, not in scale).....	4
Figure 1-2 Concrete Fracture Models .....	8
Figure 1-3 Concrete Tension Softening Models .....	10
Figure 1-4 Q8AXI Element (TNO DIANA, 2010) .....	11
Figure 1-5 CT12M Element (TNO DIANA, 2010).....	11
Figure 1-6 L6BEN Element (TNO DIANA, 2010) .....	12
Figure 1-7 CQ16M Element (TNO DIANA, 2010) .....	12
Figure 2-1 Sketch of the Direct Tension Test (Li et al., 2002) .....	16
Figure 2-2 Secant Method (TNO DIANA, 2010).....	17
Figure 2-3 Analytical Model of the Direct Tension Test in DIANA .....	18
Figure 2-4 Load-Displacement Response, Mesh I vs. Mesh II .....	19
Figure 2-5 Sketch of the Experiment by (Carpinteri et al., 1992) .....	21
Figure 2-6 Arc-Length Method (TNO DIANA, 2010).....	22
Figure 2-7 Analytical Model of the Specimen in DIANA.....	23
Figure 2-8 Comparison of the Results Obtained using Different Softening Functions with the Experiment Results.....	23
Figure 2-9 Comparison of the Results from Mesh-I and Mesh-II with the Experiment for Exponential Softening .....	24
Figure 2-10 Cracking Patterns for Mesh I and Mesh II with Different Softening Functions .....	25
Figure 2-11 Effect of the Young's Modulus (E) and the Fracture Energy ( $G_f$ ) on the Behavior .....	26
Figure 2-12 Melen Dam and the Dam Model (Binici et al., 2012) .....	28
Figure 2-13 Analytical Model in DIANA.....	29
Figure 2-14 Comparison of the Base Shear Time Histories.....	30

Figure 2-15 Comparison of the Base Shear Crest Displacement Graphs.....	31
Figure 2-16 Cracking Schemes after Pushover Analyses.....	32
Figure 2-17 Base Shear-Top Displacement Graph .....	32
Figure 2-18 Dam Model (Tinawi et al., 2000).....	33
Figure 2-19 Input Acceleration (Tinawi et al., 2000).....	34
Figure 2-20 DIANA Dam Model.....	35
Figure 2-21 Cracking Scheme for FPAs of 0.94g and 0.98g.....	37
Figure 2-22 DIANA Models with Different Mesh Densities .....	38
Figure 2-23 Final Crack Length at the Downstream Notch for Fixed $f_t$ or $G_f$ .....	39
Figure 2-24 Cracking Scheme for Different $f_t$ - $G_f$ Combinations for Model 1 .....	40
Figure 2-25 Cracking Scheme for Different $G_f$ for Model 2 .....	42
Figure 2-26 Cracking Scheme for Model 3 .....	43
Figure 2-27 Comparison of the Final Crack Length Obtained with Different Time Steps.....	44
Figure 2-28 Comparison of Response Quantities with Total Strain Fixed & Rotating Crack and Multi-Direction Fixed Crack Models .....	46
Figure 2-29 The Variation of the Final Crack Length and the Crack Opening with Shear Retention Factor .....	48
Figure 2-30 Response Quantities Obtained Using Different Damping Ratios .....	49
Figure 3-1 Concrete Gravity Dam Model.....	54
Figure 3-2 Mode Shapes.....	55
Figure 3-3 Acceleration Response Spectra (Scaled at $T_1$ ) for the Selected Ground Motions .....	59
Figure 3-4 Cracking Schemes from the IDA .....	60
Figure 3-5 Crack Zones and Cracking Schemes .....	65
Figure 3-6 First Cracked Period of the Dam.....	66
Figure 3-7 Total Crack Length of the Dam vs. Different Intensity Measures .....	67
Figure 3-8 Total Crack Length of the Dam with the Proposed Intensity Measure ....	68
Figure 3-9 Total Lateral Load Distribution for the Pushover Analysis.....	71
Figure 3-10 A Schematic Drawing of the Pushover Loading Directions.....	71
Figure 3-11 Cracking Scheme of the Pushover Analyses .....	72
Figure 3-12 IDA vs. Pushover Analyses Results .....	73

## LIST OF TABLES

### TABLES

Table 2-1 Crack Length Variation for Exponential Softening with Different E and $G_f$ .....	26
Table 2-2 First Five Natural Frequencies (Hz).....	36
Table 2-3 Maximum Stresses of the Models.....	41
Table 3-1 Selected Ground Motions.....	58



## CHAPTER 1

### INTRODUCTION

#### 1.1 General

Throughout the history, dams have been constructed for various reasons. In the ancient times, they were built for water supply and irrigation purposes. Today, many dams are being built for water supply, flood control, irrigation, navigation, sediment control and hydropower (ICOLD, 2013). Dams can be divided into two categories according to the type of the material which they are constructed: namely concrete and embankment dams. Concrete dams can further be categorized by their structural systems, i.e. concrete gravity dams, concrete arch dams and concrete buttress dams. Earth and rock fill dams and concrete faced rock fill dams make up the embankment dams (Yanmaz, 2006). In Turkey, before 2000's most of the dams were built as earth or rock fill dams; however, this trend has reversed in the last decade. Very few embankment dams have been built in the last 10 years; concrete dams are generally preferred over embankment dams (Yılmaztürk, 2012).

A concrete gravity dam, by definition, is a wide concrete berm that resists the hydrostatic forces by its geometry, weight and material strength. They are commonly preferred because of the fast construction and cost savings associated with smaller geometries. They can be built on a site where there is a strong foundation to bear the weight of the dam. In plan, most of the time, these dams are straight. If conditions are suitable, concrete gravity dams can be very tall, sometimes as high as 285 m (Grande Dixence Dam) (Ali et. al., 2012).

Çubuk 1 Dam is the first concrete gravity dam built in Turkey (1936). Some other examples of the concrete gravity and the concrete arch/gravity dams are Porsuk (1948), Sarıyar (1956), Karakaya (1987) and Berke Dams (1999). (DSİ, 2013)

As explained before, one of the reasons for the building dams is to obtain hydropower. In some countries such as Norway, Democratic Republic of the Congo and Brazil, over 90% of the electric power are supplied by the hydroelectric resources by year 1998 (ICOLD, 2013). However, at the end of 2009, less than 20% of the energy production in Turkey is provided by hydroelectric power. Therefore, in order to increase the hydroelectric power production in Turkey, investments have been made since 2006, which significantly accelerated the design and construction process for many hydropower projects (Yılmaztürk, 2010).

## **1.2 Literature Review**

The concerns about the seismic safety of concrete dams have been increasing in the last decade with the design and construction of new dams as well as the need for the evaluation the existing dam stock which were built inadequate from the seismic point of view. Shih Kang Dam failed in Taiwan due to earthquake and two dams were severely damaged due to ground excitations: Hsinfengkiang Dam in China and Koyna Dam in India (Nuss et al., 2012). Therefore, all existing dams in seismic regions and the new dams to be built should be seismically analyzed to satisfy the required performance level under severe earthquake excitations (NRC, 1990).

In order to investigate the performance of concrete gravity dams under ground excitations, linear elastic analyses are generally preferred in the literature, based as much on the historical development of the analyses methods as well as the frequency dependent nature of the dam-rock-reservoir interaction behavior. The pioneering works in this regard were conducted by Chopra and his coworkers by analyzing concrete gravity dams using two dimensional linear elastic methods (Chopra and Gupta, 1981; Hall and Chopra, 1982; Fenves and Chopra, 1985). The behavior of the

dam under earthquake excitation was determined to be significantly affected by the dam-foundation-reservoir interaction, compressibility of the water and the hydrodynamic pressure wave absorption. These analyses were conducted in the frequency domain due to the importance of the simulation of the ingoing-outgoing waves in the reservoir as well as the rock foundation.

When a dam is subjected to a severe earthquake, the stresses occurring in the dam can exceed the strength, which will cause the dam to go beyond its elastic limit, leading to significant structural damage (Asteris and Tzamtzis, 2003). This phenomenon can be investigated by nonlinear analysis procedures. The nonlinear analyses account for the tensile cracking in concrete and the resultant change in the stiffness of the system (Araujo and Awruch, 1998).

In order to examine the cracking of concrete gravity dams, many studies were made using nonlinear analyses. The two most commonly studied dams are the Koyna Dam and the Pine Flat dam (Figure 1-1). Koyna Dam was severely damaged during the Earthquake of December 11, 1967 (Çalayır and Karaton, 2005): the cracking scheme obtained from the nonlinear analyses was compared to the cracking scheme that had occurred so that the capability of the crack models to simulate the real cracking was investigated. The first study to analyze the Koyna Dam by nonlinear analysis is Pal (1976). In this study, the effect of the reservoir was neglected and the foundation was assumed to be rigid. The analyses were made using the smeared crack model, which is explained in the proceeding section. Further studying of the cracking scheme in this work shows that the results were biased due to the mesh selection, a common pitfall of using cracking models in FE analyses (Pal, 1976). Bhattacharjee and Leger (1994) studied the cracking scheme of the Koyna Dam by nonlinear analyses with smeared cracking model and rigid foundation assumption taking the reservoir effect into account. The full reservoir condition and the overflow pressure were considered. The cracking obtained in their study was in good correlation with the real cracking of the dam. Three dimensional models were also used for investigation of the behavior of the Koyna Dam. Using a smeared cracking model and a rigid foundation, along with modeling the dam-reservoir interaction, Mirzabozorg and Ghaemian (2005) obtained a cracking scheme which was in a good agreement with the real cracking of

the dam. The cracking profile for the Pine flat dam was studied by El-Aidi and Hall (1989), and Fenves and Vargas-Loli (1988) (Mansouri et al., 2011). It was observed that in a similar pattern to the Koyna Dam, the cracking occurred at the base of the dam and at the part where there is a change in slope profile.

As given above, a vast number of studies have been made to assess the cracking scheme of dams having a slope-change in their profile (Figure 1-1). The change in the slope profile leads to a stress concentration at that location prescribing the start of a crack, mostly near the crest of the dam. However, this phenomenon also leads to a bias in the analyses: this crack and its propagation always takes over the analyses and defines the final failure state. In this study, a cross section bereft of any slope changes were examined in order to understand the performance of such a dam without being biased by such a geometric detail assuring a failure at that location (Figure 1-1).

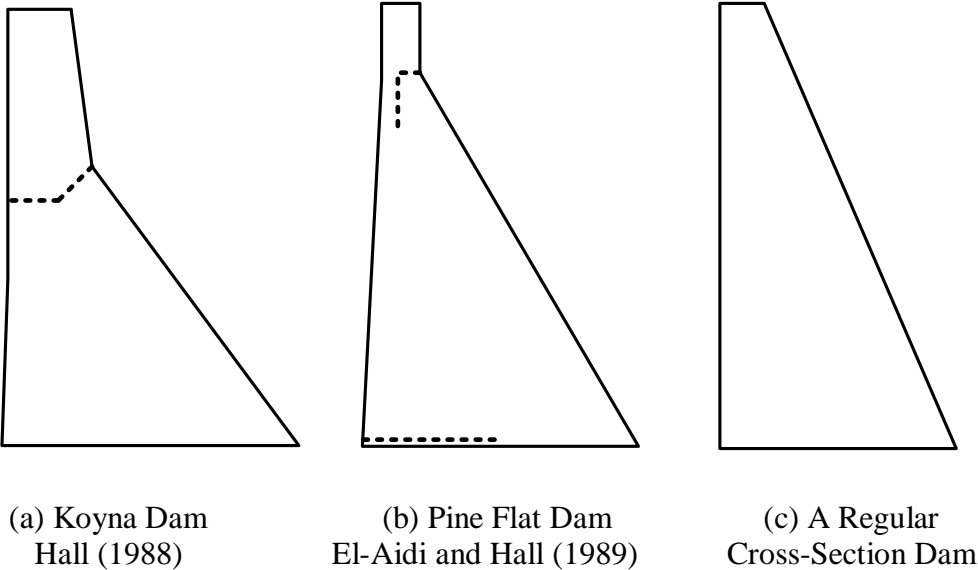


Figure 1-1 A Schematic Drawing for the Dam Cross-Sections, (the dotted lines show the cracking, not in scale)

The research on the cracking schemes of the concrete gravity dams has mostly been focused on 1) the prediction of the performance of Koyna or Pine Flat Dams and 2) the validation of cracking models for monolithic concrete, of which these structures as well as some test specimens are typical examples. However, the extreme limit states of gravity dams have not been studied, in contrast to the significant research effort for buildings in the last 3 decades for the determination of the limit states to enable performance based design (Freeman et al., 1975; Fajfar 2000; Hasan et al., 2002; Chopra, 2004). Jiang and Du (2012) investigated the cracked Koyna Dam to assess the stability of the block detached from the top of the dam finding out a large safety margin for the rigid body motion of the block. Depending on the orientation of the crack, five to eight times of the experienced Koyna earthquake could render the sliding of the top block. Pekau and Zhu (2006) performed a study on the sliding of blocks within a cracked dam. Sliding at the base and a crack at some height of the dam was found to reach 4 cm: however, it is very hard to decide on a performance limit based on this value even in the analysis methodology and earthquake uncertainty was assumed to be treated “correctly”. Incremental dynamic analysis can also be used in order to determine the limit states of the dams similar to buildings. Alembaghari and Ghaemian (2012) performed IDA on the Pine flat dam to assess the limit states and the capacity of the dam, proposing an adhoc lateral force distribution for the static pushover analysis that considers not only the inertial loads but also the hydrodynamic loads. The relation between the peak crest displacement (seismic demand parameter) and the spectral acceleration, peak ground acceleration and peak ground velocity (intensity measures) were obtained. The crest displacement and the dissipated energy were chosen as damage measures, however, a clear relation between these parameters and intensity levels were not provided. A prediction about the level of cracking does not appear to be one of the goals of this study.

For the nonlinear modeling of gravity dams, some aspects of the exact simulation of the dam-rock-reservoir interaction have to be forgone. Given the inability to conduct linear analyses, hence to obtain foundation impedance properties defining the wave transfer within the rock, the foundation has to be modeled as massless or with a finite element mesh having transmitting boundaries (Ghanaat and Chudgar, 2007) or

perfectly matched layers (Basu and Chopra, 2003). The frequency dependent dam-reservoir interaction is usually taken into account via the added mass approach introduced by Westergaard (1933). The alternative is to use a large mesh with absorbing boundaries that would enable the waves within the reservoir to travel away from the dam. Given the computational demand for these models, as well as the numerical difficulties with absorbing boundaries, an added mass approach for hydrodynamic effects and a massless foundation model is usually used in the time domain for simulation of the nonlinear behavior of dams. This approach is extensively used in the design and evaluation of dams in the literature (Leger and Boughoufalah, 1989; USACE, 2003; Chuhan et al., 2009)

Accordingly, in this study the foundation is modeled by the simplified approach introduced in USACE (1995). The foundation is modeled as a massless mesh, so that the only contribution is to the stiffness matrix and the applied ground motions will reach the dam body without any change. For hydrodynamic forces, Westergaard's added mass approach is used (Westergaard, 1933) neglecting the compressibility of the reservoir water. The hydrodynamic forces in the upstream direction are calculated by Equation 1-1.

$$p = \frac{7}{8} \rho \ddot{u}_g \sqrt{H(H-z)} \quad (1-1)$$

In this equation,  $p$  is the hydrodynamic pressure at elevation  $z$ , where  $z$  is measured from the bottom of the dam,  $\rho$  is the water density,  $\ddot{u}_g$  is the ground acceleration and  $H$  is the reservoir elevation.

### 1.3 Concrete Constitutive Modeling

Concrete fracture models can be divided into two categories as discrete crack and smeared crack models (Figure 1-2). In the discrete crack model, the crack is modeled as a geometrical discontinuity, while in the smeared crack model; the cracked solid is analyzed as a continuum (Rots, 1988).

The discrete crack model was first introduced by Ngo and Scordelis (1967) in order to model the dominant cracks within a concrete continuum. In this model, the cracks are simulated by the separation of the nodes, which led to some disadvantages: The change in the nodal connectivity of the finite element model after each crack does not fit the nature of the finite element displacement method (Rots, 1988). Furthermore, since the cracking has to be constrained along the element edges, it introduces a mesh bias (de Borst et al., 2004). This crack model is suitable when the crack location is known beforehand and the cracking forms in the form of mode I fracture (Rots, 1988).

The smeared crack model for modeling concrete behavior was introduced by Rashid (1968). In this model, the minor cracks occurring (which may later form dominant cracks) because of the heterogeneous nature of the concrete were taken into account. The cracked solid maintains its continuum (i.e. the FE mesh is not altered) and the crack model is described via the stress-strain relationship. It is assumed that the behavior of the uncracked concrete follows the isotropic stress-strain law and upon cracking, it obeys the orthotropic law, where the orthotropy axes are determined based on the crack initiation. This model has several advantages over the discrete crack model: Since the cracked solid is still a continuum, the topology of the finite element mesh is unaltered. Moreover, orientations of the cracks are not predetermined since the axes of orthotropy can change. Because of these reasons, in this study, the smeared crack model is used in the finite element simulations. Smeared crack model is divided into two as the multi-directional fixed crack model and the total strain crack model. Total strain crack model further decomposes into the fixed and rotating crack models, which are explained in the following section.

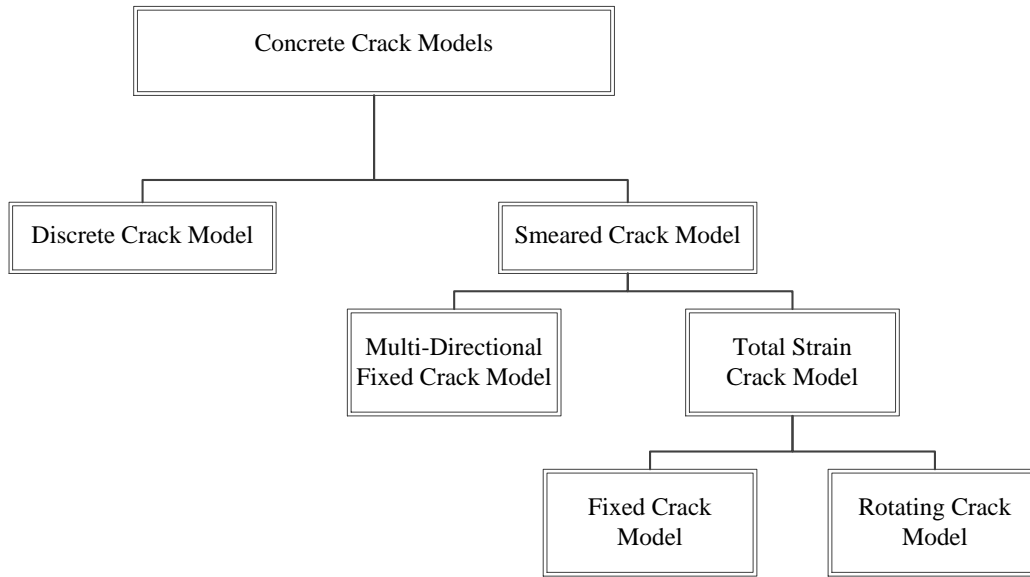


Figure 1-2 Concrete Fracture Models

### 1.3.1 Multi-Directional Fixed Crack Model

In the multi-directional fixed crack model, the total strain of concrete is decomposed into the uncracked concrete strain and the crack strain. Therefore, the crack strain can further be decomposed for each individual crack and each crack is assigned a coordinate system. This further sub-decomposition enables a number of cracks to occur simultaneously. In this model, cracking occurs when the principle tensile stress exceeds the tensile strength and the angle between an existing crack and the current principle stress direction exceeds a threshold angle. Therefore, the formation of non-orthogonal cracks is enabled. In a two dimensional setting, the orthotropic stress-strain relationship is presented below in Equation 1-2 (Rots, 1988).

$$\begin{bmatrix} \Delta\sigma_{xx} \\ \Delta\sigma_{yy} \\ \Delta\sigma_{xy} \end{bmatrix} = \begin{bmatrix} \frac{\mu E}{1-\nu^2\mu} & \frac{\nu\mu E}{1-\nu^2\mu} & 0 \\ \frac{\nu\mu E}{1-\nu^2\mu} & \frac{E}{1-\nu^2\mu} & 0 \\ 0 & 0 & \frac{\beta E}{2(1+\nu)} \end{bmatrix} \begin{bmatrix} \Delta\varepsilon_{xx} \\ \Delta\varepsilon_{yy} \\ \Delta\varepsilon_{xy} \end{bmatrix} \quad (1-2)$$

In the above equation,  $E$  is the Young's Modulus,  $\nu$  is the Poisson's Ratio,  $\mu$  is the reduction factor for mode I and  $\beta$  is the shear retention factor.

### 1.3.2 Total Strain Crack Model

Fixed crack and rotating crack models constitute the total strain crack model. Unlike the multi-directional fixed crack model, the strain is decomposed only for the cracked and uncracked concrete in the total strain crack model; the crack strain is not further decomposed. In this model, in an integration point only two orthogonal cracks can form. The crack is initiated based on the principle tensile stress exceeding the tensile strength. In the total strain fixed crack model, the orientation of the crack remains unchanged, while in the total strain rotating crack model, the orientation of crack is updated continuously and the coaxiality between the principal stress and strain is preserved. The tangential stress-strain relationship for the total strain rotating crack model in the two dimensional setting is presented in Equation 1-3 (Rots, 1988).

$$\begin{bmatrix} \Delta\sigma_{xx} \\ \Delta\sigma_{yy} \\ \Delta\sigma_{xy} \end{bmatrix} = \begin{bmatrix} \frac{\partial\sigma_{xx}}{\partial\varepsilon_{xx}} & \frac{\partial\sigma_{xx}}{\partial\varepsilon_{yy}} & 0 \\ \frac{\partial\sigma_{yy}}{\partial\varepsilon_{xx}} & \frac{\partial\sigma_{yy}}{\partial\varepsilon_{yy}} & 0 \\ 0 & 0 & \frac{\sigma_{xx}-\sigma_{yy}}{2(\varepsilon_{xx}-\varepsilon_{yy})} \end{bmatrix} \begin{bmatrix} \Delta\varepsilon_{xx} \\ \Delta\varepsilon_{yy} \\ \Delta\varepsilon_{xy} \end{bmatrix} \quad (1-3)$$

### 1.3.3 Post-Peak Response

The post-peak softening response of concrete can be modeled using different tension softening functions, namely brittle, linear, exponential and Hordyk (Rots, 1988). These functions show different behavior after reaching the tensile strength of concrete (Figure 1-3). In the brittle tension softening function, the load carrying capacity drops immediately after the tensile strength is reached, while in linear,

exponential and Hordyk models the load carrying capacity drops according to the fracture energy ( $G_f$ ) and the finite element size ( $h$ ), as shown in Figure 1-3.

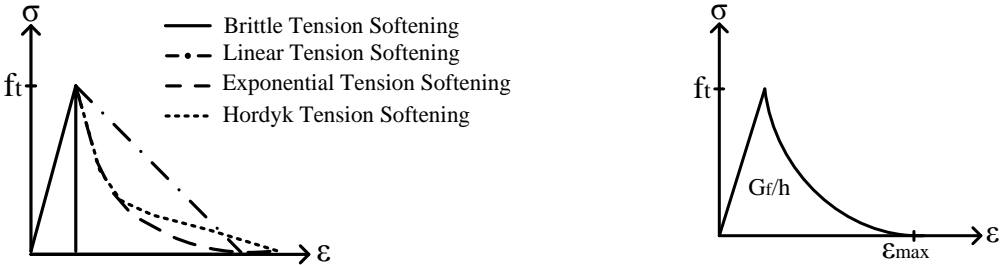


Figure 1-3 Concrete Tension Softening Models

**1.4 Finite Element Model and the Element Library**

The general purpose finite element program DIANA (Displacement Analyzer) was used as the simulation tool in this study. The software allows nonlinear transient analyses with 2D, 3D, plane-strain, plane-stress as well as axisymmetric elements. A range of elements were used within the analyses performed in this study, such as the four-node isoparametric element Q8AXI, the six node isoparametric plane stress element CT12M, the two-node isoparametric beam element L6BEN and the eight node isoparametric element CQ16M (TNO DIANA, 2010). Some details on the elements used in the study are provided below.

**1.4.1 Q8AXI Element**

Q8AXI is a four-node isoparametric axisymmetric solid ring element having a quadrilateral cross-section (Figure 1-4). The unknowns are the translations in the nodes in the global x and y directions. This element has linear shape functions (TNO DIANA, 2010).

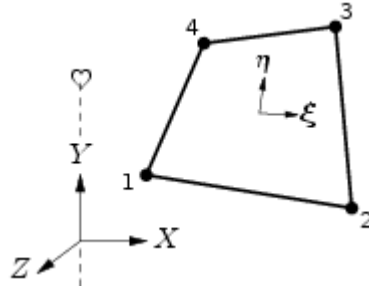


Figure 1-4 Q8AXI Element (TNO DIANA, 2010)

The displacements,  $u_i$ , at the nodes in x and y directions are approximated by Equation 1-4 (TNO DIANA, 2010).

$$u_i(\xi, \eta) = a_0 + a_1\xi + a_2\eta + a_3\xi\eta \quad (1-4)$$

#### 1.4.2 CT12M Element

CT12M is a six-node triangular isoparametric plane stress element with quadratic shape functions (Figure 1-5). The unknown translational displacements,  $u_i$ , at the nodes are approximated by Equation 1-5 given below (TNO DIANA, 2010).

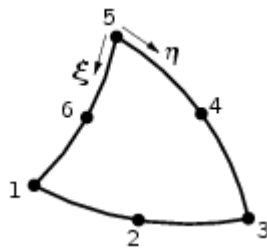


Figure 1-5 CT12M Element (TNO DIANA, 2010)

$$u_i(\xi, \eta) = a_0 + a_1\xi + a_2\eta + a_3\xi\eta + a_4\xi^2 + a_5\eta^2 \quad (1-5)$$

**1.4.3 L6BEN Element**

L6BEN is a two-node, two-dimensional beam element (Figure 1-6). The unknown displacements in the x-direction,  $u_x$  and in the y-direction,  $u_y$  are calculated by Equation 1-6 demonstrated below (TNO DIANA, 2010).

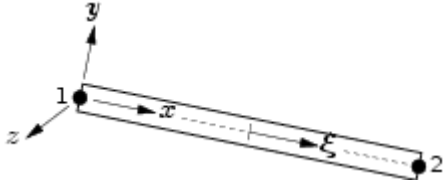


Figure 1-6 L6BEN Element (TNO DIANA, 2010)

$$\begin{aligned}
 u_x(\xi) &= a_0 + a_1 \xi \\
 u_y(\xi) &= b_0 + b_1 \xi + b_2 \xi^2 + b_3 \xi^3
 \end{aligned}
 \tag{1-6}$$

**1.4.4 CQ16M Element**

CQ16M is an eight-node quadrilateral isoparametric plane stress element with quadratic shape functions (Figure 1-7). The unknown translational displacements,  $u_i$ , at the nodes are approximated by Equation 1-7 presented below (TNO DIANA, 2010).

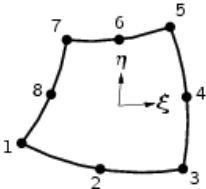


Figure 1-7 CQ16M Element (TNO DIANA, 2010)

$$u_i(\xi, \eta) = a_0 + a_1\xi + a_2\eta + a_3\xi\eta + a_4\xi^2 + a_5\eta^2 + a_6\xi^2\eta + a_7\xi\eta^2 \quad (1-7)$$

## 1.5 Objectives and Scope

Many dams are being built in seismically very active locations in valley ridges very close to major fault lines. These sites, which were avoided in the past for more preferable locations are actively being realized as the possible locations for hydropower location are increasingly scarce. Moreover, most of the dam stocks in the developed world were built for lower seismic risk than currently prescribed for new structures in these countries. Many of these systems are older than 40-50 years, in which period our knowledge about the fault systems as well as procedures for determining/predicting earthquake levels increased significantly. Consequently, although no gravity dam system has ever been fully tested within design ground motion levels, such as Loma Prieta, Chi Chi and Koyna Earthquakes, significant risk exists (Nuss et al., 2012). Such a ground motion can lead to a significant damage on a dam, far from its elastic peak response, requiring nonlinear analyses to assess the performance of the dam. In contrast to the experience in linear analyses, the nonlinear behavior and performance limits of dam monoliths are not well known.

The primary goal of this study is to investigate the nonlinear behavior of a typical 80 m high concrete gravity dam monolith in this regard.

The quantification of damage on a dam monolith is a cumbersome task. In order to properly address this issue, the following steps were taken:

- ❖ The damage wrecked on a system by earthquakes is very much time history dependent. Therefore, using a range of ground motions, the possible development of cracks and the typical cracking schemes in such a monolith was investigated.
- ❖ Extensive cracking on the dam body significantly changes the period of the structure, therefore an investigation of the cracking of the dam body on the fundamental period of the system was conducted.

- ❖ Given that the cracking on the system is dependent on the ground motion characteristics, a relationship between the cracking and the earthquake ground motion characteristics were sought. As the cracking on a dam body can be expressed as a dam measure, this relationship can also be expressed as a preliminary design tool to assess expected damage on a system from an earthquake.
- ❖ The IDA analyses conducted are computationally very expensive and time-consuming. Therefore, similar to reinforced concrete buildings, pushover analysis was used to investigate the performance limits of the dam body. A comparison of pushover analyses with the IDA results was performed to investigate the effectiveness or suitability of this approach to the response prediction of a dam monolith.

For the sake of brevity, the study as mentioned above is presented in only three chapters in this thesis. First, the preliminary information and the validation study on the material models used are presented in Chapter 2. The calibration of the constitutive model for the material to four different experimental studies focused on gravity dams is presented. The results of the IDA analyses are presented in Chapter 3 along with pushover analysis results. The relationship between seismic demand and intensity measures are computed and presented in this chapter. In Chapter 4, the conclusions from this study and future avenues of research on this topic are summarized.

## CHAPTER 2

### CALIBRATION TESTS

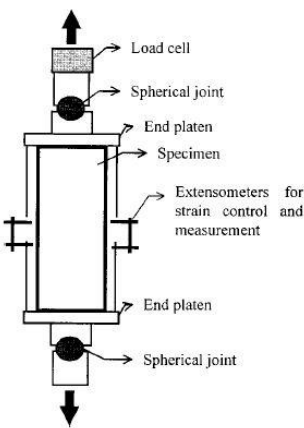
#### 2.1 Introduction

Calibration is the process of adjusting the properties of an analytical model in order to match a set of experimental results obtained in the laboratory. It is a very important process which shows that a mathematical model is capable of reproducing physical phenomenon, and can be used henceforth as a prediction tool. In this study, the general purpose finite element program DIANA was used in the analyses. In order to investigate the capabilities of the program and use it as a prediction tool, a set of calibration studies were conducted for laboratory experiments conducted with different types of loading. Four works from the literature were selected to investigate capabilities of DIANA for the simulation of concrete gravity dams under seismic loading. The first of the chosen benchmark experiments was the roller compacted concrete (RCC) direct tension test conducted by Li et al. (2002) performed under static conditions. The second benchmark study was the experiments conducted by Carpinteri et al. (1992) on a model concrete gravity dam under lateral loading in static conditions. The third benchmark study is the pseudo dynamic testing of concrete dams by Binici et al. (2012). The last benchmark study used is a detailed shake table testing study on a scaled model of a concrete gravity dam conducted by Tinawi et al. (2000).

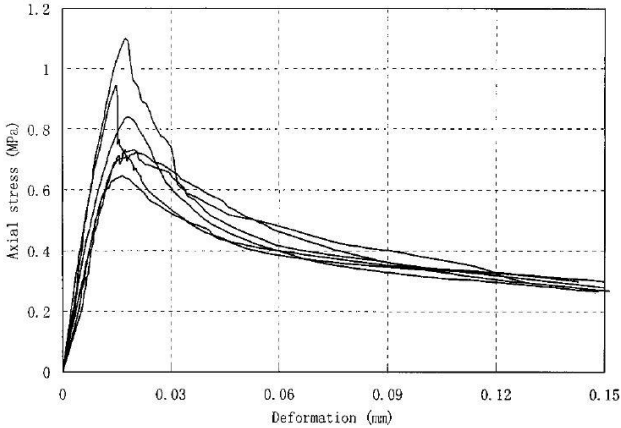
### 2.2 Analytical Simulation of Direct Tension Tests

In their experimental study, Li et al. (2002) tested cylindrical RCC cores obtained from an RCC dam under uniaxial direct tension. The RCC cores were obtained from the RCC matrix and the interface. They tested two categories of specimens with different compressive strengths to examine the effect of compressive strength. Furthermore, to investigate the effect of specimen size, two groups with different sizes of specimens were tested. A total number of 28 specimens were tested having different characteristics such as the tensile strength, peak strain and fracture energy. The main goal of the experiment was to obtain the complete stress-deformation curves of the specimens (Figure 2-1). Moreover, some relationships between the specimen characteristics and the mechanical properties were proposed by the authors. The experiment was displacement controlled: the sketch of the test setup is presented in Figure 2-1.

The analytical study was focused on the acquisition of complete stress-deformation curve. Therefore, one specimen from the RCC matrix was selected for the analysis. Another aspect of this study was to obtain the fracture energy correctly.



(a) Experimental Setup



(b) Stress-Deformation Curve

Figure 2-1 Sketch of the Direct Tension Test (Li et al., 2002)

For the analytical modeling in DIANA, the specimen labeled as T-17 by Li et al. (2002) was selected. The size of the specimen was 150x300 mm. The compressive and tensile strengths were 15 MPa and 1.10 MPa, respectively. The modulus of elasticity was given as 23.6 GPa and the fracture energy 263 N/m.

Four-node isoparametric axisymmetric elements (Q8AXI) were used in this study (TNO DIANA, 2010). The bottom nodes were restrained in the x and y directions while the top nodes were restrained in the y direction for the application of loading. In order to prescribe the location of cracking, tensile strengths of elements 5 and 13 were reduced by 1%. An initial displacement was applied to the top nodes of the model and increased incrementally throughout the analysis. Total strain rotating crack model with the predefined Hordyk tension softening (TNO DIANA, 2010) was used in the analyses. The analyses were conducted satisfying both the force and displacement converge criteria (at 0.01) using 1000 load steps. Secant method was used in the analyses, in which the secant stiffness matrix is derived for each loading stage (Figure 2-2 TNO DIANA, 2010).

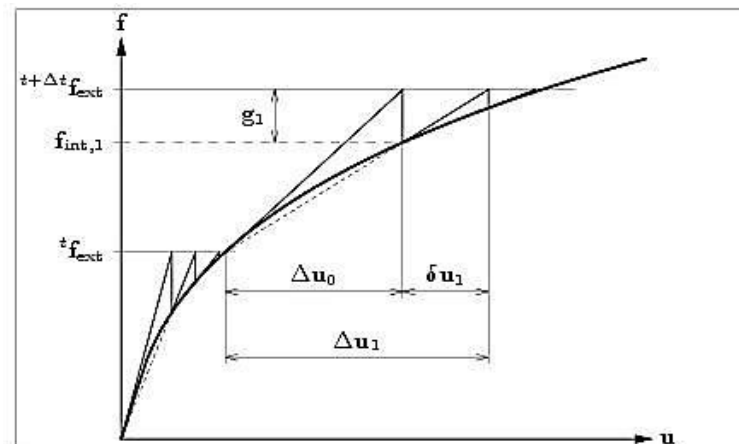
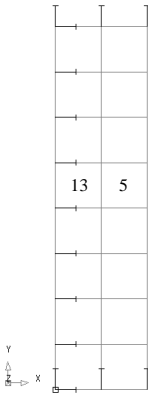


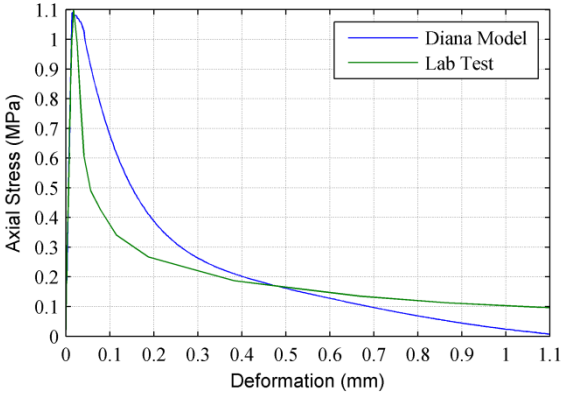
Figure 2-2 Secant Method (TNO DIANA, 2010)

The 16 element model used for the simulation and the results of the analyses are presented in Figure 2-3. The area under the axial stress deformation curve yields the fracture energy (Li et al. 2002). In order to obtain the prescribed fracture energy, 263

N/m, the “effective” element size,  $h$ , in the DIANA model had to be prescribed since this variable is assumed as 1 by default for axisymmetric elements in DIANA. The area under the ‘DIANA Model’ curve in Figure 2-3 was calculated as 254 N/m, which is very close to the stated fracture energy 263 N/m. The effective element size to be used in the material model was determined to be  $0.4a$  for square elements with side length  $a$ . The comparison of the axial stress-deformation response from Li et al. (2002) and the DIANA model, as shown in Figure 2-3, show that the post-peak response of the model, as modeled with Hordyk softening, was satisfactory for this test, albeit unable to catch the initial sudden drop in the resistance of the specimen.



(a) Finite Element Mesh



(b) Stress-Displacement Curve

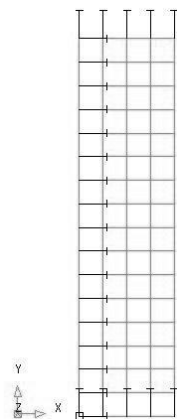
Figure 2-3 Analytical Model of the Direct Tension Test in DIANA

**2.2.1 Investigation of the Effect of Mesh Density**

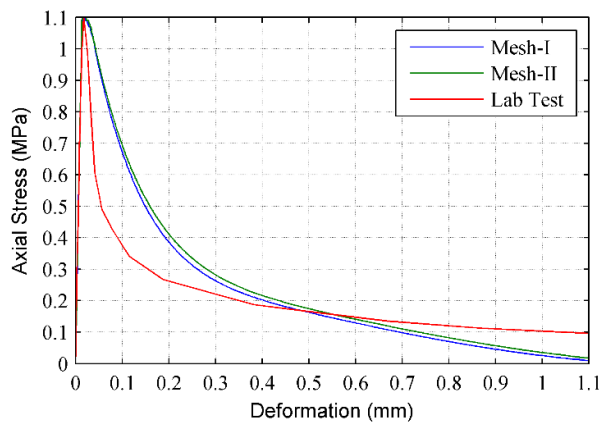
Mesh density is regarded as a critical part of the modeling of the behavior of concrete structures given that the early analyses in this field were observed to be largely biased by mesh dependence. The concentration of the cracking in concrete to singled out locations renders the modeling of displacements by continuous displacement functions, such as in the finite elements, a significant challenge. Mesh dependence is usually addressed using the crack energy concept (Bazant, 1986): a formulation used

in DIANA as well. However, even with this formulation, the modeling and accurate prediction of displacements for bulk concrete structures is still an issue with the post-peak response determining the displacement behavior and crack propagation.

In order to study the effect of mesh density on the analyses, the analyses given above (16 elements, Mesh I) were re-conducted with a different finite element mesh consisting of 64 elements (Mesh II, Figure 2-4). For the second mesh (Mesh-II), a higher load step of 4000 was used and the element size was reduced to 0.007. Similar to Mesh I, the effective element size was found as 0.37a. The fracture energy was calculated as 270 N/m. The comparison between Mesh-I, Mesh-II and the test by Li et al. (2002) is presented in Figure 2-4.



(a) Analytical Model with 64 Elements



(b) Comparison, Mesh I-II

Figure 2-4 Load-Displacement Response, Mesh I vs. Mesh II

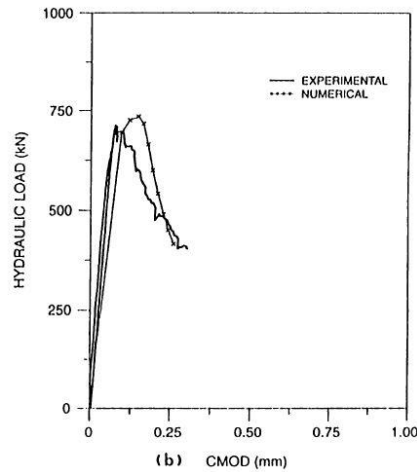
It can be concluded from Figure 2-4 that increasing the mesh density did not affect the response significantly. The results obtained were not biased by the mesh chosen for the analyses. For this case, dividing the model into more elements necessitated a

significant increase in the number of load steps leading to much higher computational cost.

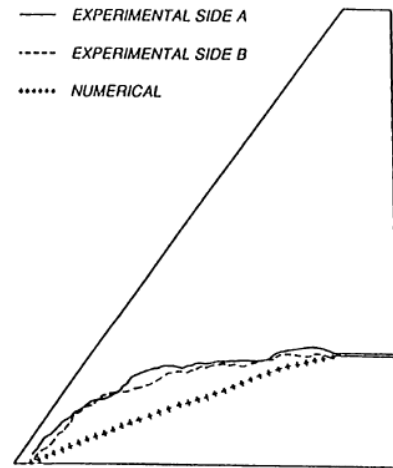
### **2.3 Analytical Simulation of a Notched Model Concrete Dam**

Carpinteri et al. (1992) tested two small scale (1:40) concrete gravity dams under hydrostatic loading. The height of the specimens was 2.4 m with 0.03 upstream and 0.7 downstream slopes. A horizontal notch was prepared in the upstream face at 60 cm from the base of the dam in order to determine the initiation point for cracking: the depths of the notches were 15 and 30 cm for the first and second models, respectively. Three tests were conducted on these two specimens. The experiments were displacement controlled using the crack mouth opening displacement (CMOD) at the notch as the controlling parameter. The first two tests were conducted on the same specimen due to an unexpected cracking at the bottom of the specimen observed in the first test during the application of additional loads before hydrostatic loading. The experiment was repeated (the second test) after the repair of the model and the test was conducted under the aforementioned hydrostatic loading. Finally, the third test was conducted on the second specimen only under hydrostatic loading; the self-weight simulation was not conducted. The relationship between the total applied force and CMOD was obtained for these experiments along with the cracking profile on the specimens.

In their study, Carpinteri et al. (1992) also performed finite element analyses of the experiments using the discrete cracking model. In the simulations, they assumed the modulus of elasticity as 35.7 GPa, Poisson's Ratio as 0.1, tensile strength as 3.6 MPa and the fracture energy as 184 N/m. The comparison of the analytical and experimental results from Carpinteri et al. (1992) is given in Figure 2-5 for the third test.



(a) Force vs. CMOD Graph (Carpinteri et al., 1992)



(b) Cracking Profile (Carpinteri et al., 1992)

Figure 2-5 Sketch of the Experiment by (Carpinteri et al., 1992)

The experiment of Carpinteri et al. (1992) was used in this section in order to validate the performance of the utilized material model.

### 2.3.1 Investigation of CMOD Displacement

The modeling of the experiment (third test only) was conducted using a plane stress model. Eight-node quadrilateral elements, CQ16M and six-node triangular elements, CT12M (TNO DIANA, 2010) were used in the analyses. The notch in the specimen was predefined in the model by removing the necessary elements at its location. Similar to the experiment conducted by Carpinteri et al. (1992), the analyses were displacement controlled and arc-length method formulated in (TNO DIANA, 2010) was used (Figure 2-6) with CMOD control at the crack mouth (displacements of the nodes at the opposite sides of the notch). The arc-length method constrains the norm of the incremental displacements in a load-stepping analysis and hence the post peak behavior and unloading can be simulated correctly (TNO DIANA, 2010). Two different mesh structures, namely, medium (Mesh-I) and dense (Mesh-II) were

utilized to investigate the dependence of the results on the finite element mesh. Four different tensile softening functions, namely brittle, exponential, Hordyk and linear (TNO DIANA, 2010) functions were used in order to investigate the effect of the shape of the post-peak concrete response on the analyses results.

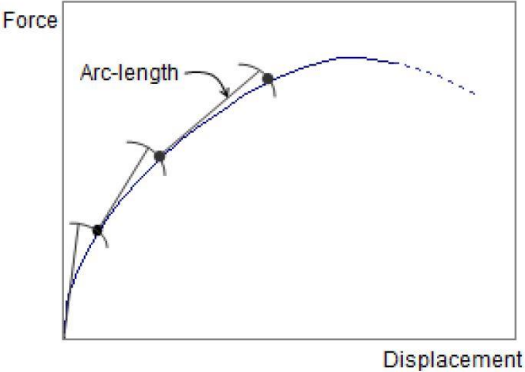


Figure 2-6 Arc-Length Method (TNO DIANA, 2010)

Mesh I consisted of 669 CQ16M elements and 26 CT12M as given in Figure 2-7. Total strain rotating crack model was utilized in the analyses. In order to overcome the initial low stiffness and capacity of the model, the modulus of elasticity was increased by 1.58 and the fracture energy by 1.36.

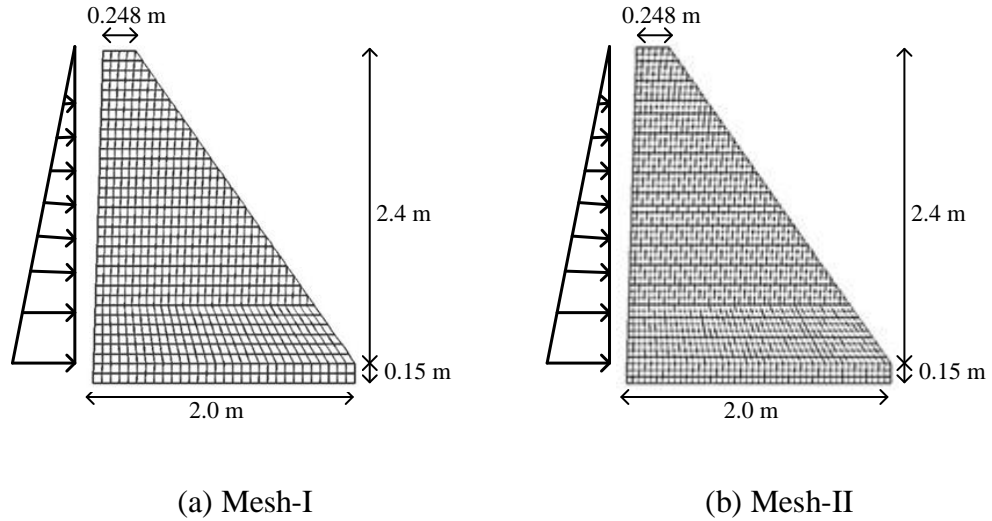


Figure 2-7 Analytical Model of the Specimen in DIANA

For mesh I, the behavior of the models with different post-peak softening functions is presented in Figure 2-8 along with the experimental data. Linear tension softening function appears to over predict the peak response while the Hordyk model under predicts the peak. Brittle response results in a very significant under prediction of the capacity of the monolith since no fracture energy is specified. It can be concluded from Figure 2-8 that the behavior is best represented by the linear and exponential tension softening functions.

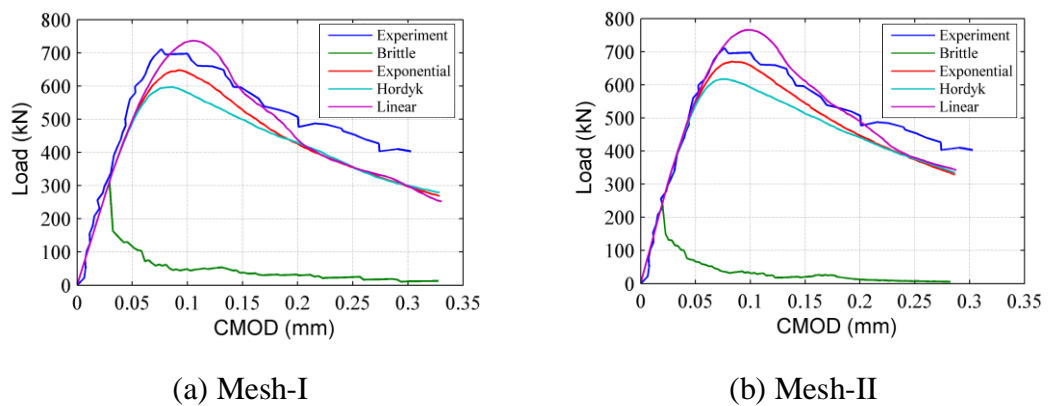


Figure 2-8 Comparison of the Results Obtained using Different Softening Functions with the Experiment Results

A much denser mesh was used for the second set of analyses simulating the experimental test of Carpinteri et al. (1992). This mesh (Figure 2-7) was composed of 1464 CQ16M and 39 CT12M elements. The comparison of tension softening functions together with the experimental data is given in Figure 2-8. The results obtained from Mesh II appear very similar to their counterparts from Mesh I (Figure 2-8). Exponential and linear tension softening functions yielded the closest result to the experiment.

The most significant effect of the increase in the mesh density appears to be the better representation of the initial stiffness for the second model. A direct comparison of the analyses conducted with exponential tension softening models for the different meshes are presented in Figure 2-9, showing that initial stiffness is better estimated for the denser mesh and the capacity of the specimen is incrementally better estimated.

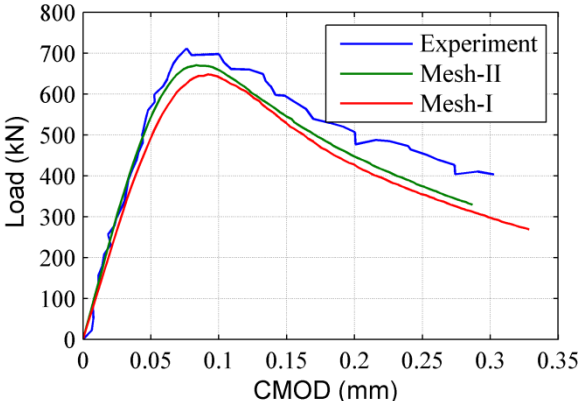


Figure 2-9 Comparison of the Results from Mesh-I and Mesh-II with the Experiment for Exponential Softening

### 2.3.2 Investigation of Cracking Pattern

The effect of the material model on the development and propagation pattern of the cracking within the analytical model was also investigated. For the above mentioned four softening functions and two different mesh structures, Figure 2-10 shows the cracking pattern of the model dam, where the red line shows the cracking observed in the experiment of Carpinteri et al. (1992). The crack length was estimated very similarly for the exponential, Hordyk and linear softening functions, while the brittle softening function yielded significantly larger cracking in the specimen. However, this softening function failed to simulate the peak load for the CMOD behavior of the model as mentioned above.

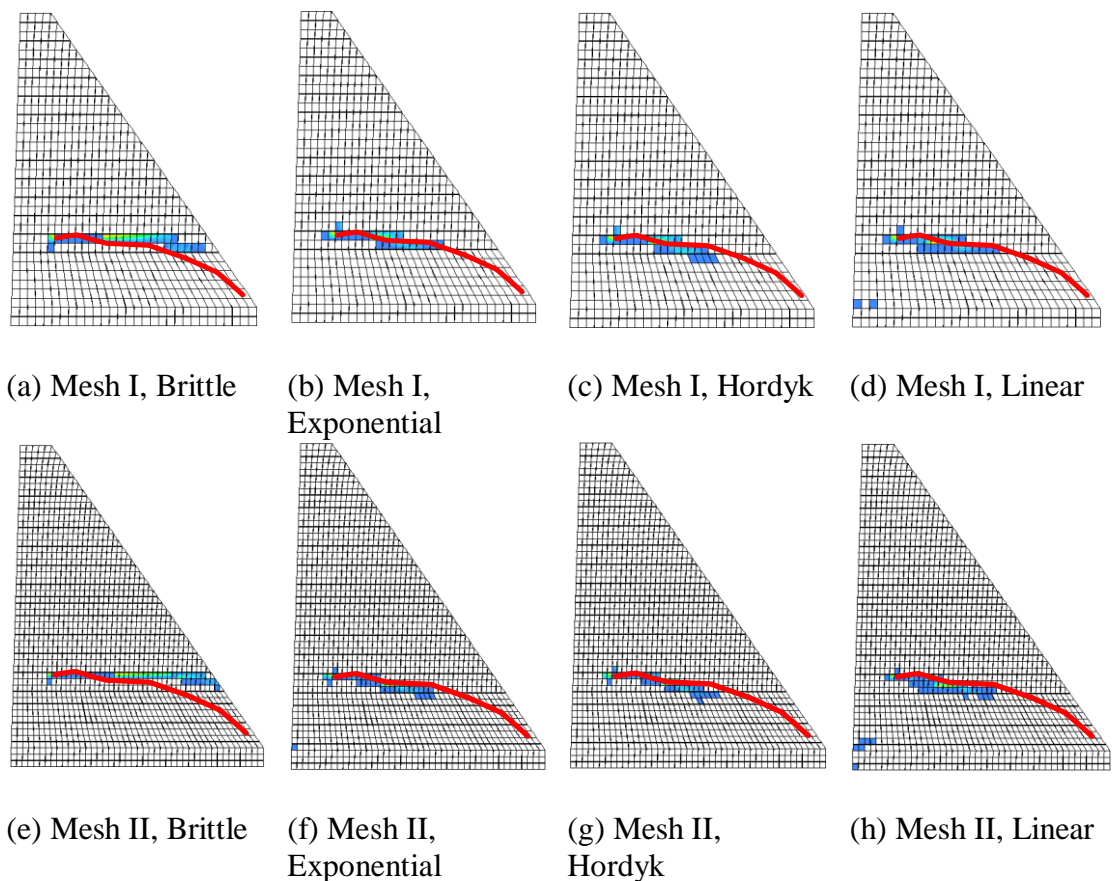
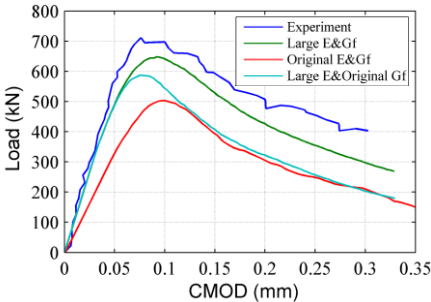


Figure 2-10 Cracking Patterns for Mesh I and Mesh II with Different Softening Functions

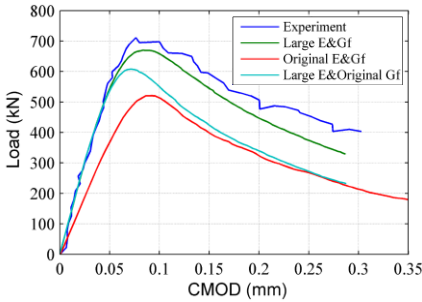
As given above, the crack length predicted by the models (~1.0 m) were less than the actual cracking observed in the experiment by Carpinteri et al. (1992) (1.6 m), although the CMOD vs. load was estimated well. The results were similar to those obtained in an analytical model by Bhattacharjee and Leger (1994) using two different cracking models reporting crack lengths of 1.1 and 1.2 m. As explained before, the analyses given above were conducted increasing the Young's Modulus and the fracture energy. The Young's Modulus and the fracture energy both effect the propagation of the crack significantly. A set of analyses were then conducted in order to investigate the effects of these two parameters on the crack length and the dam behavior. The variation of the crack length and the load-CMOD graph with these parameters are presented in Table 2-1 and Figure 2-11, respectively.

Table 2-1 Crack Length Variation for Exponential Softening with Different E and  $G_f$

	Young's Modulus	Fracture Energy	Crack Length (m)
<b>Mesh I</b>	1.58x	1.36x	0.9
	1.00x	1.00x	1.12
	1.58x	1.00x	0.95
<b>Mesh II</b>	1.58x	1.36x	0.84
	1.00x	1.00x	1.03
	1.58x	1.00x	0.91



(a) Mesh I, Different E and  $G_f$



(b) Mesh II, Different E and  $G_f$

Figure 2-11 Effect of the Young's Modulus ( $E$ ) and the Fracture Energy ( $G_f$ ) on the Behavior

The crack length was best estimated using the original modulus and fracture energy, which failed to reproduce the load-CMOD behavior of the experiment. An amplified Young's Modulus and fracture energy was the best combination of parameters to reproduce the load-CMOD response and to obtain the crack length similar to the work done by Bhattacharjee and Leger (1994). Given the similarity of the analytical results from all different studies, it is admissible that a factor that was not considered in these analyses resulted in the significant extension of cracking during the experiment.

#### **2.4 Pseudo-Dynamic Earthquake Simulation and Analytical Pushover Analysis**

A set of experiments were conducted at Middle East Technical University to investigate the seismic behavior of RCC dams under the supervision of Prof. Dr. Barış Binici supported by TUBITAK under the grant 111M712. The experiments were performed on a 1/75 scaled model of the 120 m high Melen Dam which was designed for water supply to the city of İstanbul. The upstream and downstream slopes were 0.15 and 0.75, respectively (Figure 2-12). Three different specimens were built in order to investigate the effect of construction material on the performance. The special setup of the test enabled the use of only the bottom half of the dam section while the inertial and load effects of the remaining part were included in the test using special loading apparatus (Figure 2-12). The first specimen was built out of regular concrete while the other two specimens were built imitating RCC construction practices with different target strengths. The thicknesses of the specimens were 20 cm, representing a plane stress setting. These models were tested under three levels of scaled earthquakes by pseudo-dynamic analysis, followed by pushover analyses leading to failure (Binici et al., 2012).

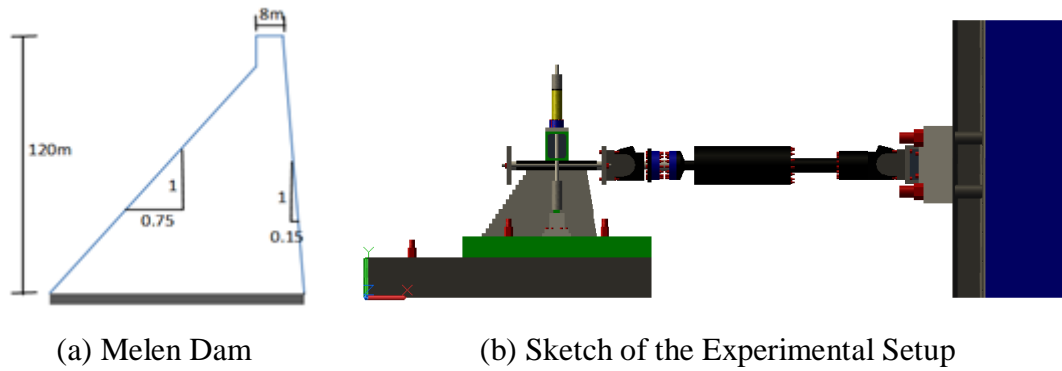


Figure 2-12 Melen Dam and the Dam Model (Binici et al., 2012)

An important point in the experiments was to obtain the base shear and the overturning moment for the scaled specimen close to the unscaled dam. Additional axial load had to be prescribed to the system in order to simulate its own weight and the hydrostatic effects. Similarly, additional mass had to be placed to simulate the inertial effect.

The first experiment conducted in the laboratory was chosen for calibration purposes in this study. The analytical dam model is presented in Figure 2-13. The dam body consisted of 500 CQ16M elements and the steel plate on top of the dam model was modeled using L6BEN beam elements. The Young's Modulus of steel plate was assumed as 200 GPa and the Poisson's Ratio as 0.3. For the dam body, the Poisson's Ratio was assumed as 0.2 and the density as  $2400 \text{ kg/m}^3$ . In order to obtain the first natural frequency of dam model at 14.3 Hz, the Young's Modulus of concrete was assumed as 12.35 GPa. In accordance with the experimental results, the tensile and compressive strengths of concrete were used as 1.95 MPa and 25 MPa, respectively (Aldemir et al., 2013). Softening functions used in the analyses were chosen as the parabolic compression softening and the exponential tensile softening. The compressive and tensile fracture energy values were assumed as 20000 N/m and 100 N/m, respectively. Analyses were conducted using the total strain rotating crack model. Simulation of the pseudo-dynamic model was conducted by applying the crest displacements measured on the specimen for three levels of earthquakes, OBE,

MDE and MCE levels, statically. Static pushover analysis was then conducted in order to determine the failure state.

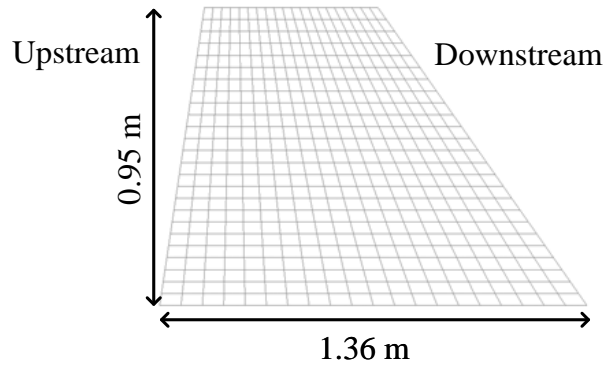
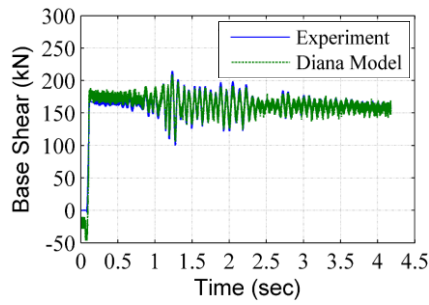


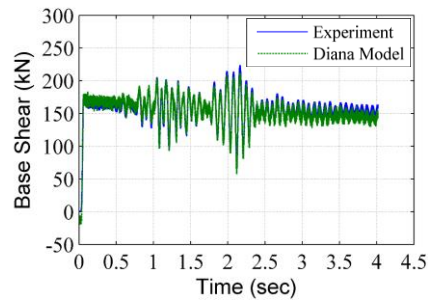
Figure 2-13 Analytical Model in DIANA

#### 2.4.1 Static Earthquake Simulation

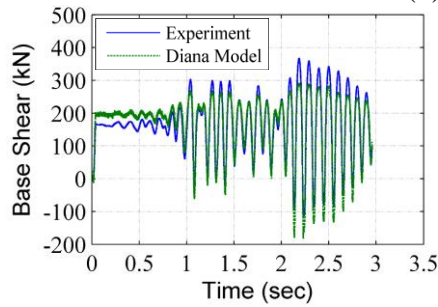
The time histories of the base shear are compared with the experimental results for the three earthquakes in Figure 2-14. The application of the crest displacements from the experiment as static loading to the crest enables eliminating the uncertainty in such tests due to the hard to prescribe damping ratio.



(a) OBE Level



(b) MDE Level



(c) MCE Level

Figure 2-14 Comparison of the Base Shear Time Histories

The results of the simulation were quite close for the OBE and MDE levels. For the MCE level event, the DIANA model estimated the base shear with a 10% error.

The base shear top displacement graphs were also compared with the experimental data (Figure 2-15). For OBE level, due to some problems in the experiment, different initial stiffness was estimated. The simulation results for MDE level were quite close to the experiment. For MCE level, however, since the cracking pattern could not be simulated correctly, the behavior was estimated different.

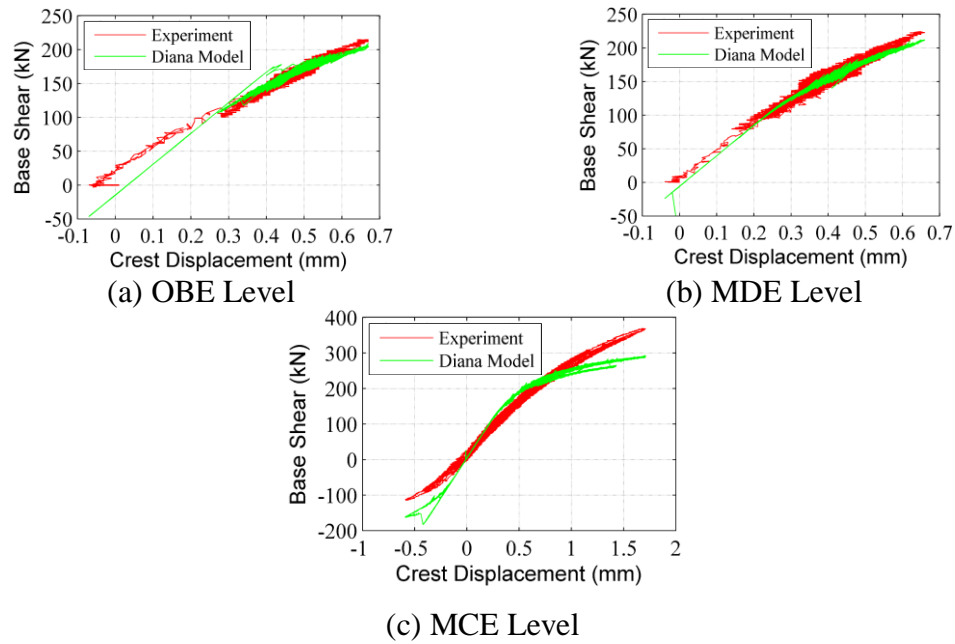


Figure 2-15 Comparison of the Base Shear Crest Displacement Graphs

#### 2.4.2 Analytical Simulation of the Pushover Experiment

Two pushover analyses were conducted by applying displacement to the crest nodes that was increased incrementally. The first analysis, referred to as Analysis 1, was conducted on the uncracked dam, while in the second analysis, referred to as Analysis 2, the crack lengths after the MCE level were taken into account. In Analysis 2, the tensile strength of elements that should be cracked due to MCE event was reduced so that cracking occurred at the beginning of the pushover analysis. The cracking schemes are presented in Figure 2-16 together with the upstream crack photograph of the experiment (Binici et al., 2012). The length of crack at the upstream face of the model was obtained as 30 cm in Analysis 2, which was in a good correlation with the experimental results, since the crack propagated in the experiment during pushover. Given the initial cracking scheme was not prescribed correctly, Analysis 1 only yielded cracking at the bottom of the specimen.

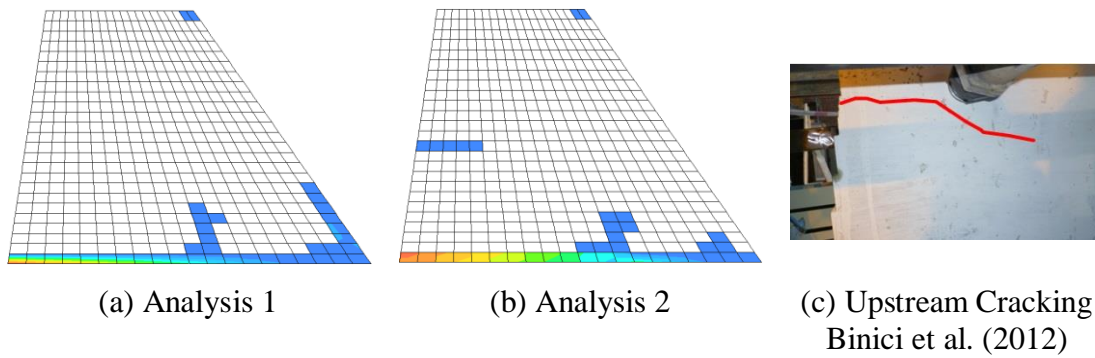


Figure 2-16 Cracking Schemes after Pushover Analyses

The base shear-top displacement behavior from the analytical study was compared to the experiment results in Figure 2-17. As can be seen from Figure 2-17, capacities were estimated similarly for the Analysis 1 and 2, governed by the base crack. However, for the Analysis 1, the top displacement capacity was underestimated.

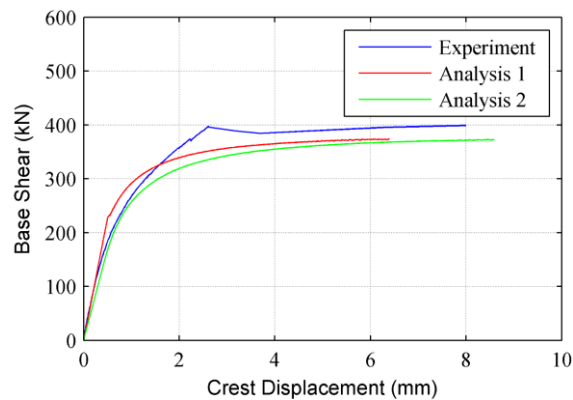


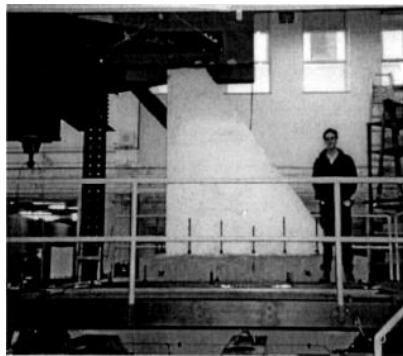
Figure 2-17 Base Shear-Top Displacement Graph

## 2.5 Analytical Simulation of Shake Table Testing on a Scaled Gravity Dam

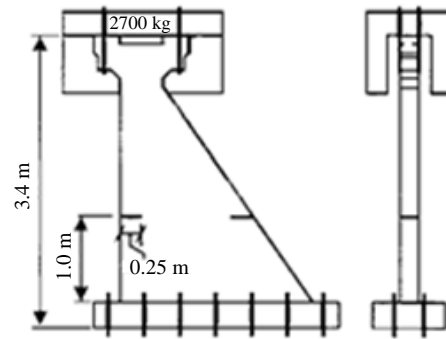
### 2.5.1 Shake Table Test and Specimen

The experimental results of Tinawi et al. (2000) was reproduced in this study using a finite element model in DIANA in order to calibrate the modeling assumptions for

the analytical simulation of the behavior of concrete gravity dams. In their experimental study, Tinawi et al. (2000) tested a plain concrete gravity dam monolith having a height of 3.4 m. The upstream side of the monolith with a thickness of 0.25 m was vertical while the downstream side was built 1V/0.7H. Two notches having a thickness of 10 mm and a length of 250 mm were made in order to prescribe the location of the crack on the monolith. A 2700 kg mass was placed at the crest so that the natural frequency of the system was reduced. The photograph and a sketch of the specimen that was tested are presented in Figure 2-18.



(a) Photograph of the Dam Model



(b) Sketch of the Dam Model

Figure 2-18 Dam Model (Tinawi et al., 2000)

In the experiment, the specimen was subjected to triangular acceleration pulses, which was reflected as the excitation function given in Figure 2-19 due to the trouble with the control of the shake table. This pulse was scaled with respect to its first peak acceleration (FPA) to three different values: 0.87, 0.94 and 0.98g. It should be noted that the second peak was greater than the first peak acceleration. The tests with the FPA of 0.94g and 0.98 are referred as the first and second cracking tests, respectively (Tinawi et al., 2000). The first test with the FPA of 0.87 did not lead to any cracking on the specimen.

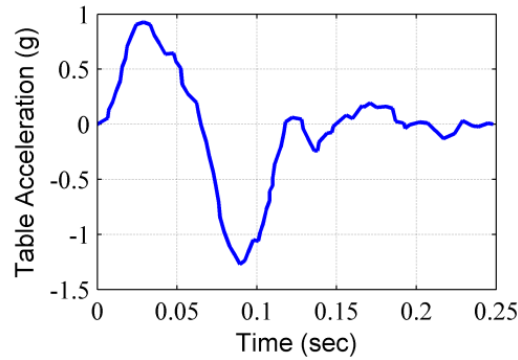


Figure 2-19 Input Acceleration (Tinawi et al., 2000)

### 2.5.2 Analysis Results

The specimen was modeled in a plane stress setting with a mesh size of approximately 9 cm, corresponding to 695 CQ16M elements and 14 CT12M elements, as given in Figure 2-20. The attached masses and the beam system for attaching the mass were accurately reflected in the model in order to simulate the mass distribution of the system properly. The notches in the specimen were predefined in the model by removing the necessary elements at its location. Stiffness proportional Rayleigh damping was used in the study. In accordance with Tinawi et al. (2000), the damping ratio in the analyses was assumed as 1% and 10% in the first mode of the structure, respectively, for the first and second cracking tests.

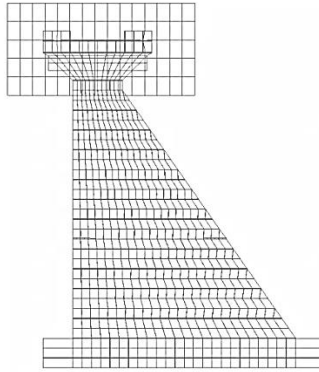


Figure 2-20 DIANA Dam Model

As mentioned above, during the testing, some problems with the shaking table were observed caused by the inherent flexibility of the shake table in the vertical axis. In order to consider the effect of the flexibility of the table, 7 individual springs were modeled at the base of the DIANA model, similar to the analytical Model M2 used by Tinawi et al. (2000). The stiffness values of the springs were set to 230 kN/mm so as to obtain the first natural frequency of the test setup correctly. The foundation stiffness selected as such was higher than the selection by Tinawi et al. (2000). The natural frequencies obtained henceforth are compared to the empirical results and analytical model M2 from Tinawi et al. (2000) in Table 2-2. DIANA model was more successful in yielding a close estimation of the first five modes compared to the model by Tinawi et al. (2000). Both models had difficulty in reproducing the vertical vibration mode of the system (mode 2).

Table 2-2 First Five Natural Frequencies (Hz)

	<b>Laboratory Test Tinawi et al. (2000)</b>	<b>Model M2 Tinawi et al. (2000)</b>	<b>DIANA Model</b>
<b>f<sub>1</sub></b>	16.4	16.4	16.33
<b>f<sub>2</sub></b>	30.0	-	-
<b>f<sub>3</sub></b>	60.0	57.5	63.23
<b>f<sub>4</sub></b>	105.0	72.0	103.14
<b>f<sub>5</sub></b>	150.0	145.3	146.93

For the nonlinear analyses, the modulus of elasticity and the compressive strength values were assumed in accordance with Tinawi et al. (2000) as 14.8 MPa and 14.8 GPa, respectively. In order to enable cracking in the first cracking test, tensile strength was set to 3.25 MPa and the brittle tension softening model was used. Tensile strength was amplified by 1.53x in order to consider the strength increase due to dynamic loading, in contrast to 1.75x amplification used by Tinawi et al. (2000). For the shake table test with an FPA of 0.87g, no cracking was obtained in the model. Increasing the FPA incrementally, in accordance with Tinawi et al. (2000), a partial crack in the downstream notch was obtained for the first cracking test for FPA= 0.94g. A complete crack joining the upstream and downstream notches were obtained for the second cracking test with FPA= 0.98g. The cracking schemes for both tests are compared with the experimental results of Tinawi et al. (2000) in Figure 2-21.

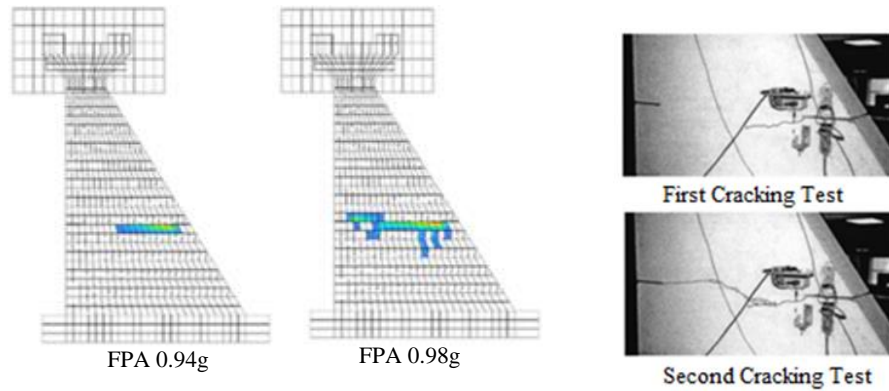


Figure 2-21 Cracking Scheme for FPAs of 0.94g and 0.98g

### 2.5.3 Investigation of the Effect of Modeling Parameters on the Crack Location and Propagation

Mesh density and the material parameters used are the primary factors affecting the development of the cracking on the specimen. In order to consider the effect of mesh density, the dam was modeled with three different element sizes of approximately 5 cm, 10 cm and 15 cm (Figure 2-22), referred to as Model 1, Model 2 and Model 3, respectively. Models 1, 2 and 3 were composed of 1671, 717 and 520 CQ16M elements, respectively. The material parameters affecting the propagation of the crack can be summarized as the properties of the softening curve, the fracture energy and the tensile strength of the material.

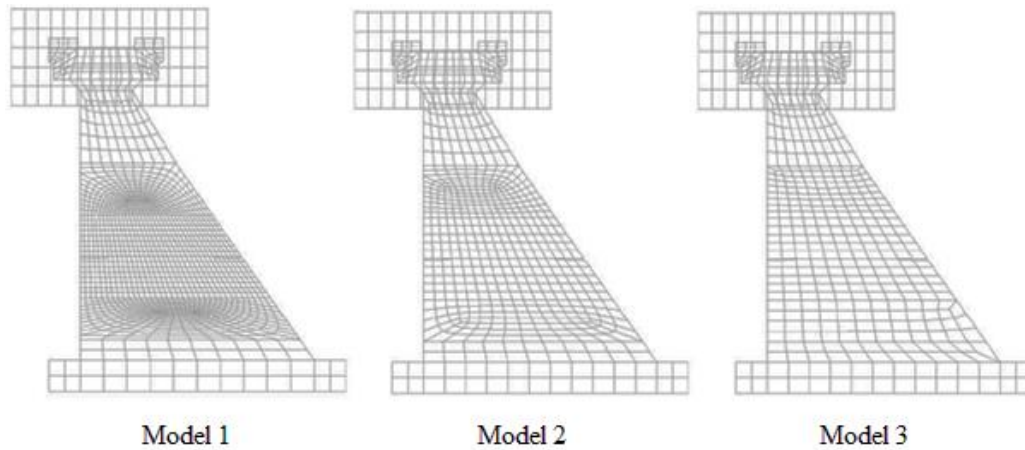
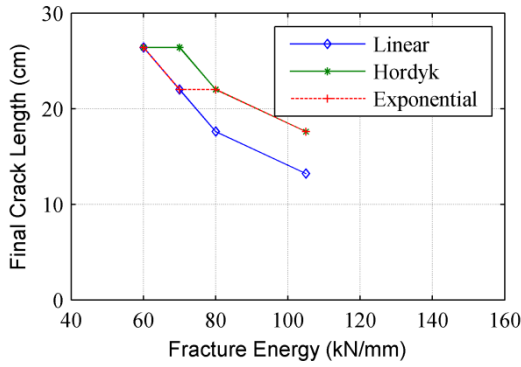


Figure 2-22 DIANA Models with Different Mesh Densities

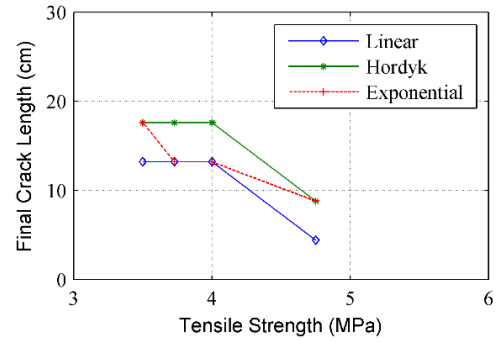
### 2.5.3.1 The Effect of Tension Softening Functions and Fracture Energy

The final crack length for the first and second cracking test were studied considering the effect of the softening curve of the material in this section using model 1 with a dense mesh structure. As before, a set of seven springs were modeled at the base of the dam models to obtain the first frequency of the system at 16.4 Hz. The foundation stiffness of the model was the same as the one modeled by Tinawi et al. (2000).

The post-peak response as well as the fracture energy of the concrete was observed to significantly change the propagation of the cracking during the shaking of the specimen. The effect of the prescribed fracture energy on different post-peak response models were investigated first keeping the tensile strength of the model at 3.73 MPa and modifying the fracture energy. As shown in Figure 2-23a, the fracture energy significantly changes the propagation behavior with the linear softening model displaying the highest sensitivity to this parameter. An increase tensile strength keeping the fracture energy constant also significantly reduced the amount of crack propagation in the analytical model, as shown in Figure 2-23b. Increase in any one of these parameters changed the length of crack propagation preventing the crack to reach the experimental observation of 30 cm.



(a)  $f_t=3.73$  MPa



(b)  $G_f=105$  kN/mm

Figure 2-23 Final Crack Length at the Downstream Notch for Fixed  $f_t$  or  $G_f$

The effect of the softening curve can also be observed from Figure 2-23. For both combinations, Figure 2-23a and b, the crack length is obtained the smallest when linear tensile softening function was used, followed by the exponential model. Hordyk tensile softening led to the highest crack propagation among the models. The post-peak slope of the Hordyk model appears to be very effective in defining the length of the propagation of the crack.

The crack propagation and scheme were in good correlation with the test results by Tinawi et al. (2000). However, the correct cracking scheme was obtained using two different combinations of the fracture energy and the tensile strength, such as combination 1 with the tensile strength 4.5 MPa and the fracture energy 60 kN/mm and combination 2, with the tensile strength 2.4 MPa and the fracture energy 105 kN/mm. The cracking schemes for both combinations are presented in Figure 2-24. The inverse problem obviously has more than one solution and the shape of the softening curve and the tensile strength can be varied with respect to each other to obtain similar crack propagation between the upstream and downstream notches. However, the cracking behavior for the first cracking test was different: the first combination reproduced the results of that test as well as the second one.

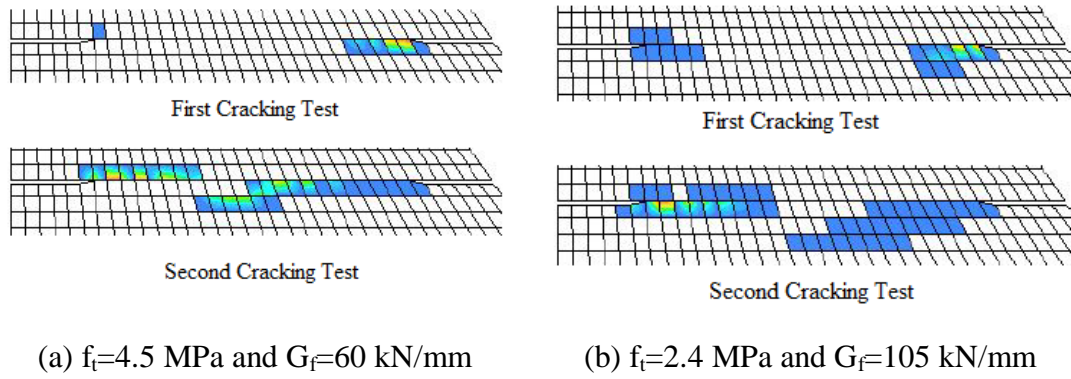


Figure 2-24 Cracking Scheme for Different  $f_t$ - $G_f$  Combinations for Model 1

Finally, it can be concluded that cracking was significantly affected by both the tensile strength and the fracture energy defining the softening curve of the concrete. The propagation of the crack observed in the second test can be reproduced by applying dynamic application factor to either the tensile strength or the fracture energy. Amplifying both of the values led to less crack penetration.

### 2.5.3.2 The Effect of Mesh Density

The different mesh structures as given in Figure 2-22, fine (Model 1), medium (Model 2) and coarse (Model 3) meshes, were utilized to determine the effect of a selected mesh density on the crack propagation within the analytical model. The spring stiffness values were assumed as 193 kN/mm, 205 kN/mm and 210 kN/mm each, for the Models 1, 2 and 3, respectively. Elastic analyses were conducted to obtain the maximum tensile stress at the tips of upstream and downstream notches. The results are tabulated in Table 2-3.

Table 2-3 Maximum Stresses of the Models

Model 1		Model 2		Model 3	
Max. Stress (MPa)		Max. Stress (MPa)		Max. Stress (MPa)	
Upstream Notch	Downstream Notch	Upstream Notch	Downstream Notch	Upstream Notch	Downstream Notch
4.04	5.54	2.81	3.81	2.76	3.42

As given in Table 2-3, the stress generated near the edge of the notch increased as the element size decreased. When the mesh became denser, there was a significant increase in the stress concentration at the notch leading to an increase in the stress demand. The issue was significantly more problematic in model 1; due to the nature of the very fine mesh, very large stress concentrations were forming near the discontinuity (the notch), leading to unexpected cracking, such as the cracking observed in the upstream notch for the first cracking test. Therefore, the model had to be biased towards large tensile strengths due to this issue, which is a common, well-known problem for solution of continuum problems with finite elements. Analyses were also conducted with high values of tensile strength and fracture energy of 4.5 MPa and 300 N/m, respectively, which still led to cracking near the notches that did not propagate into the rest of the model.

Given that the stress near a discontinuity is theoretically near infinity, the finite element model tries to approach to the theoretical solution when the element size is decreased. However, the cracking occurs due to effect of stresses on an effective area, not the point of discontinuity. This is a limitation of the macro-modeling of the concrete which is very heterogeneous in nature. As well as setting a limit on the maximum element size, a limit should also be abided on the minimum element size. Significantly more information on the limitations on the macro modeling of concrete are provided in Bazant (1986). The minimum element size is a valid limitation to the modeling of this specimen, because of its small size and the presence of notches yielding stress concentrations. When dynamic analyses were repeated on a model without a notch, a similar mesh bias was not observed. Within the limits of the

current computational power, however, the minimum element size, which is specified as three times the maximum aggregate size (Bazant, 1986), is not a limit for the large dam monoliths as we cannot use as fine a density of mesh for these systems.

The analyses of the model 2 and 3 were performed using exponential tension softening with 1% and 4% stiffness proportional Rayleigh Damping for first and second cracking tests, respectively. Total strain rotating crack model was used in the analyses. For Model 2, the crack penetration was reproduced with a tensile strength of 3.73 MPa and a fracture energy of 80 kN/mm (Figure 2-25). These values were very close to their counterparts assumed in the analytical study by Tinawi et al. (2000). Reducing the fracture energy slightly (60 kN/mm), a similar cracking scheme was obtained as given in the same figure, leading to the overestimation of the cracking in the first test. Crack mouth opening was estimated larger in this case, and the crest response changed significantly.

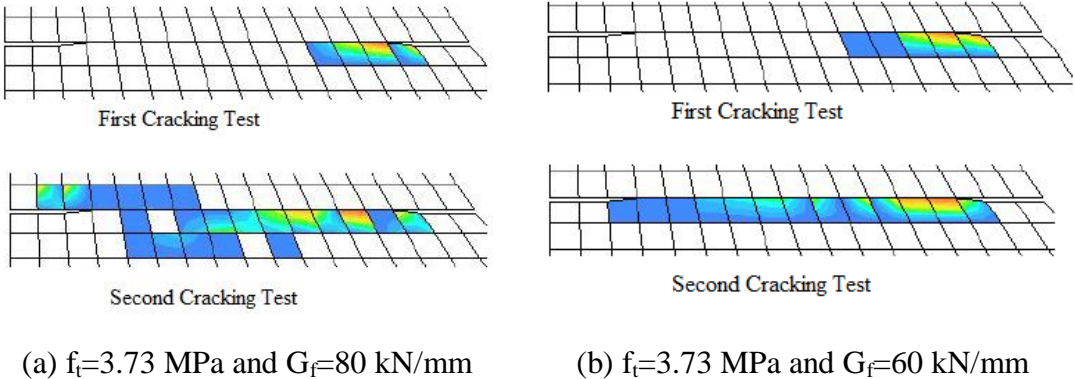


Figure 2-25 Cracking Scheme for Different  $G_f$  for Model 2

For model 3, the cracking scheme was reproduced with a tensile strength of 3.3 MPa and fracture energy of 80 kN/mm as shown in Figure 2-26. Notably, the strength of the material had to be assumed somewhat smaller in this model, as due to the coarseness of the mesh, smaller stress demand were obtained in the finite element

model. In the second crack test crack mouth opening displacement reached to a value of nearly 1 mm. It can be concluded that when crack is localized, high values of crack mouth opening displacement can be reached.

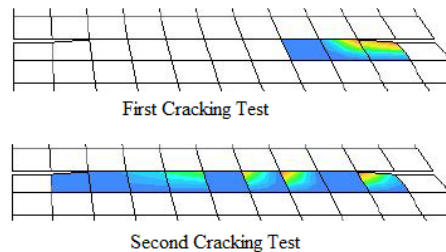


Figure 2-26 Cracking Scheme for Model 3

The three different meshes used in this section showed that the stress variation due to the finite element model is an effective quantity in determining the distribution of the cracking on concrete elements. Notably, similar fracture energies was used for all models to reproduce the cracking given in both cracking tests simultaneously, however, to correctly predict the initiation of cracking, the tensile strength has to be changed for each model, i.e. from 4.5, 3.7 to 3.3 for fine, medium and coarse meshes, respectively. These represent 2.11 times, 1.74 times and 1.55 times the static strength for the specimen. The fracture energy was used as 1.3x the static value as well. Given that models for large dam monoliths will be considered on the coarse side, the use of 1.5x the tensile strength as suggested in USACE (1995) appear reasonable for nonlinear modeling to obtain the cracking on these systems.

#### 2.5.4 The Effect of the Time Stepping Factor

Given that the duration of the pulse is very important for determining the crack propagation, the effect of time stepping on the analyses results are considered in this section. In order to investigate the effect of the time stepping factor, analyses were

conducted with five different time steps  $\Delta t$  of 0.00100, 0.00060, 0.00040, 0.00025 and 0.00005 seconds corresponding to 250, 450, 625, 1000 and 5000 steps in the analyses for reaching the total duration of 0.25 seconds. While the maximum tensile stresses generated in the dam were same for these five different analyses, for a decrease in the  $\Delta t$ , the effective duration of the maximum stress increased, leading to more cracking on the specimen. The final crack length did not change with further reduction of  $\Delta t$  from  $\Delta t=0.0004$  seconds. Reducing  $\Delta t$  to 0.00005, there was only a slight difference in the response of the dam. The effect of the time step  $\Delta t$  on the final crack length is summarized in Figure 2-27. The  $\Delta t$  used for the analyses changed the time period in which the maximum stress was effective on the system, hence for larger  $\Delta t$  values, with the reduction of effective time, the crack propagation was reduced. Consequently, the use of 1000 time steps was adequate in order to optimally represent the behavior of the dam and decrease the computational cost. It should be noted that Tinawi et al. (2000) used 5000 time steps in their analytical study. The use of  $\Delta t=0.00025$  (1000 time steps) falls towards the smaller of the limits prescribed for nonlinear transient analyses in Chopra (2007). For the fourth mode at 105 Hz,  $T_n/20$  equals 0.0005 seconds.

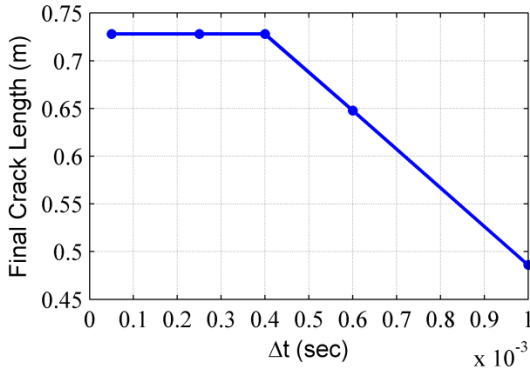


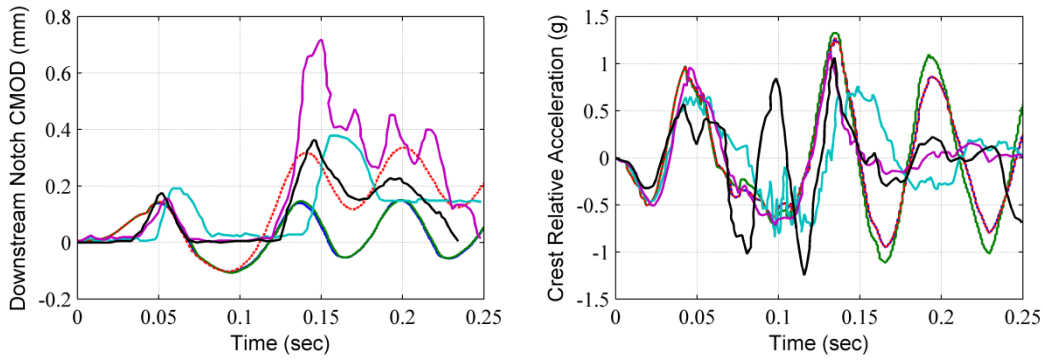
Figure 2-27 Comparison of the Final Crack Length Obtained with Different Time Steps

## **2.5.5 Detailed Investigation of the Simulation of Crack Opening**

The ability of the analytical models to reproduce the displacements from the two cracking tests was investigated in this section.

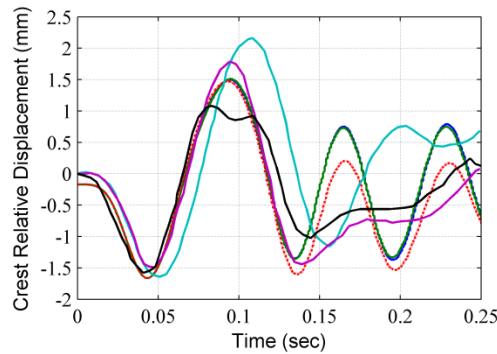
### **2.5.5.1 The Effect of the Material Modeling**

Using the total strain rotating/fixed crack and the multi-directional fixed crack model, the prediction of the displacement response of the specimen at the crack mouth was investigated in this section. The shear retention factor is nominally equal to 1 in the rotating crack model, while it was formally specified as 1.0 for the total strain fixed crack and multi-direction fixed crack model. The results obtained for the crack mouth opening at the downstream notch, the crest relative displacement and the crest relative acceleration for the total strain models are presented in Figure 2-28 for the first test. The total strain crack models yield very similar results as given in the figure. Given the test setup, which prescribed the plane of maximum principal stress well near the prebuilt notches, the models yielded very similar results. However, it can be seen these models failed to simulate the downstream notch crack mouth opening displacement after the first peak of the CMOD. A better response was obtained when the multi-directional fixed crack model was used. These results were closer to the results obtained in the analytical model by Tinawi et al (2000). In this model, the shear retention factor within the crack plays an important role, the effect of which is investigated in the following section.



(a) Downstream Notch CMOD

(b) Crest Relative Displacement



(c) Crest Relative Acceleration

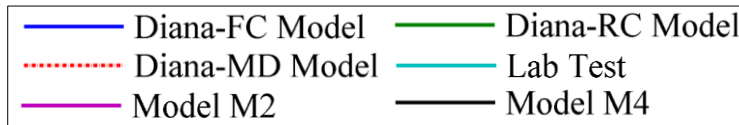


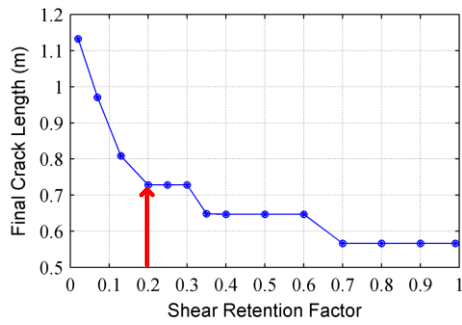
Figure 2-28 Comparison of Response Quantities with Total Strain Fixed & Rotating Crack and Multi-Direction Fixed Crack Models

### 2.5.5.2 The Effect of the Shear Retention Factor

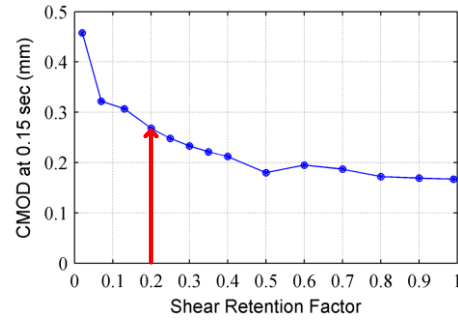
As given in Figure 2-28, the notch opening was not reproduced correctly with the total strain models for a shear retention factor of 1, prescribing full shear transfer at the crack plane after the closing of the cracks. According to Rots and Borst (1987), when there is an unsymmetrical loading, the crack will both open and slide, damaging the crack plane. A reduction in shear stiffness in terms of a shear retention factor should be taken into account. In order to model this loss in the crack plane,

fixed crack model, in a total strain or multi-direction formulation, is more appropriate. The crack opening displacement, crest displacement and the crest acceleration of the specimen are presented in Figure 2-28 for both models using a shear retention factor of  $\beta=0.2$ . The inclusion of a lower shear retention factor did not significantly affect the displacement and acceleration response for the total strain crack model, on the other hand, a satisfactory prediction of the displacement response was obtained with the multi-direction fixed crack model as shown above. However, a further complication arose for these models: reproducing the CMOD values could only be obtained with crack elongation twice as much as Tinawi et al. (2000).

The effect of shear retention factor on the crack length and the CMOD was studied using a range of shear retention factors and computing the final crack length and the CMOD at 0.15 seconds. As can be seen from Figure 2-29, the final crack length increased with a decreasing shear retention factor. The increase in the crack length also corresponded to an increase in the CMOD at  $t=0.15$  sec. These two graphs suggest the use of a shear retention factor around 0.2 in order to best represent the behavior of the specimen for the first cracking test. Although Tinawi et al. (2000) used a varying shear retention factor in the analytical modeling of the experiment in accordance with the suggestion from Rots and Borst (1987) in the form of a shear softening function, a constant shear retention factor assumed as in the DIANA analyses led to satisfactory results for matching the final crack length and the CMOD at 0.15 seconds. It can be concluded that as a general trend, when the shear capacity of the concrete decreases, the crack propagates more and CMOD increases.



(a) Final Crack Length with Shear Retention Factor

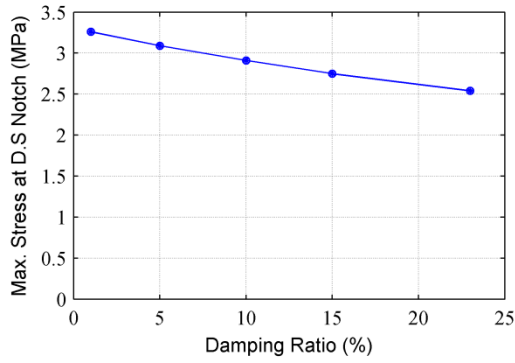


(b) CMOD at t=0.15 sec

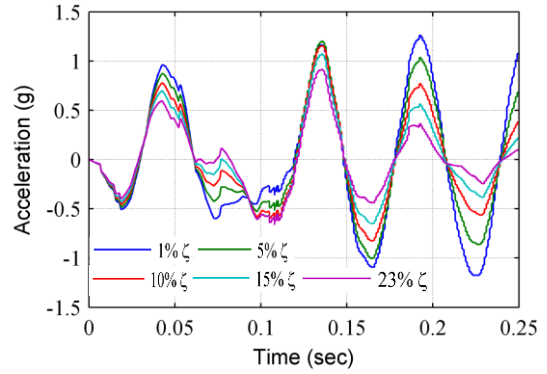
Figure 2-29 The Variation of the Final Crack Length and the Crack Opening with Shear Retention Factor

### 2.5.5.3 The Effect of Rayleigh Damping

The displacements obtained in the analyses were also seen to be sensitive to the damping prescribed to the model. Very little of the damping in the specimen occurs due to the viscous damping sources naturally prescribed in analytical solutions; majority of the damping takes place as a result of the crushing and shearing at the crack interface which significantly changes the displacement response of the monolith. A single damping ratio, at 1%, was used above, in accordance with Tinawi et al. (2000). The effect of higher Rayleigh Damping on the analysis results were investigated using 1%, 5%, 10%, 15% and 23% in a set of analyses. The maximum tensile stress generated at the tip of the downstream notch decreased with increasing damping ratio as given in Figure 2-30. A linear relationship to this reduction is discernible: the stress dropped as much as the damping was increased. The damping ratio affects the crest acceleration directly as shown in Figure 2-30.



(a) Maximum Stress at Downstream Notch



(b) Crest Acceleration

Figure 2-30 Response Quantities Obtained Using Different Damping Ratios

In order to obtain the CMOD displacements more correctly, a more detailed formulation for the damping at the crack is obviously necessary. The treatment of damping at the crack plane requires a more detailed concrete constitutive model which is left for a future study.

#### 2.5.5.4 Second Cracking Test

In the second cracking test, the results of the analytical study reproduced the crack penetrating between the two notches as found by Tinawi et al. (2000); however, the crack mouth opening displacement was obtained very small compared to the laboratory test and the crest response was obtained out-of-phase with the test. The use of different shear retention factors had no significant effect on final crack length and crack mouth opening displacement. Analyses were conducted with different damping ratios from 1% to 23% to model the second cracking test; however, damping ratio did not increase the CMOD significantly. According to Yamaguchi et al. (n.d.), the abrupt decline of the response can be modeled with transient damping only, not with Rayleigh damping for this phase of the test. Using a transient damping proportional to the instantaneous secant stiffness matrix, the decline of the response was modeled correctly, while the dam continued its harmonic motion using Rayleigh

damping. In the analytical models, Tinawi et al. (2000) used instantaneous damping as well. Kimata et al. (2008) modeled the specimen with stiffness proportional damping as a function of time, reaching similar results. As the formulation currently used does not include step by step determination of the damping component of the resisting force based on the material stiffness properties, like the secant stiffness, the displacement response of the specimen could not be reproduced properly. As mentioned above, a more detailed concrete constitutive model should be formalized for this purpose.

## 2.6 Summary

The results from the four different calibration studies are summarized as follows:

- ❖ The shape of the post-peak curve and the strength determine the crack propagation process. For all the three test, it was observed that softening functions with faster declining curves after the peak were more appropriate for use, such as Hordyk or exponential models.
- ❖ For the finer meshes approaching the limits of macro-modeling of concrete, concentration of the stresses led to significant stress demands, and required the assumption of higher tensile strength values in order to reproduce test behavior. However, within current limitations of computational power, modeling of monoliths is still well within macro modeling limits. The 1.5x dynamic strength, as prescribed by USACE (1995) appears appropriate for dynamic modeling of concrete monoliths.
- ❖ Both the rotating and fixed crack models yielded similar cracking patterns predicting the crack propagation correctly for the experiments. However, the displacement predictions were rather off the mark. Further study in constitutive modeling is required to predict accurate displacements or crack openings for monolithic concrete structures.
- ❖ Shear retention factor and the damping behavior within the crack appear to be important factors in the determination of correct crack mouth displacements.

However, these are very complex issues significantly related to aggregate interlocking, crushing within the crack, and possibly the number of cycles the cracks go through. Further testing is required in order to address these issues with a more detailed constitutive model.



## CHAPTER 3

### INCREMENTAL DYNAMIC ANALYSIS OF A CONCRETE GRAVITY DAM

#### 3.1 Introduction

In Chapter 2, it was shown that the crack length and its location in a dam can be simulated accurately in a finite element model. The analytical model as well as the total strain crack models can be used to investigate the distribution of cracking within a dam body. To this end, the nonlinear behavior of an 80 m high dam monolith was investigated in this section using incremental dynamic analysis (IDA) with the primary purpose of understanding the nonlinear performance of this structure as well as its performance limits. This chapter of the thesis is organized as follows. First, the finite element model used in the analyses is outlined, followed by a brief definition of the incremental dynamic analysis procedure used. The set of 21 ground motions used for the analyses are presented next. The analysis results are then presented, in which the relationship between key seismic intensity parameters and the seismic demand results are investigated. Finally, the results of the IDA are compared to the static pushover analysis results in order to evaluate the scope of possible use of pushover analyses for determining the performance levels of dams.

#### 3.2 Gravity Dam Model

The dam investigated in this chapter is an arbitrary concrete system, with a typical 80 m high monolith with a vertical upstream and a 0.8H/1V downstream face. The crest

length of the monolith was assumed as 6 m (Figure 3-1). As explained before, the foundation was modeled according to the simplified approach introduced in USACE (1995) and the hydrodynamic forces were accounted for by Westergaard’s added mass approach (Westergaard, 1933). The reservoir elevation was assumed at 78 m.

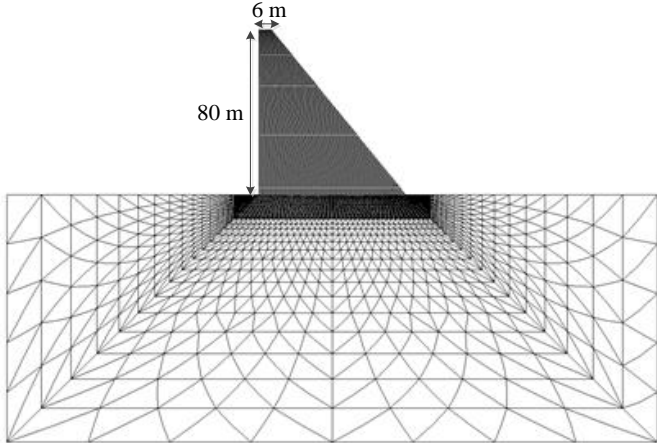


Figure 3-1 Concrete Gravity Dam Model

The analyses in this section were performed using the total strain rotating crack model. The dam body was modeled with 5025 CQ16M elements and 45 CT12M elements while the foundation was modeled with 4430 CT12M elements. The Young’s Modulus, Poisson’s ratio, density and the tensile strength for the dam monolith were assumed as 12.0 GPa, 0.2, 2400 kg/m<sup>3</sup> and 1.8 MPa, respectively. Exponential tension softening function was used with a fracture energy of 225 N/m. The use of this value for the element size given in the dam mesh was validated so that no strength reduction would occur during the analyses. It was assumed that failure would occur due to tensile overstressing (Alembagheri and Ghaemian, 2012); therefore, the crushing failure was ignored and the compressive behavior was assumed elastic. For the foundation, a medium quality rock foundation was assumed; Young’s Modulus was taken as 10.8 GPa and the Poisson’s Ratio as 0.3.

The effective damping ratio (Equation 3-1) due to the effect of the foundation and reservoir was calculated in accordance with USACE (1995) as given below. It takes the individual damping contributions of dam, foundation and reservoir into account.

$$\widetilde{\epsilon}_1 = \frac{1}{R_r} \frac{1}{R_f^3} \epsilon_1 + \epsilon_r + \epsilon_f \quad (3-1)$$

In the above equation,  $\widetilde{\epsilon}_1$  is the effective damping ratio,  $\epsilon_1$  is the damping value that is suggested to be assumed as 5% for OBE level ground motions.  $\epsilon_r$  and  $\epsilon_f$  are the added damping ratios due to hydrodynamic effects and dam-foundation interaction, respectively.  $R_r$  is the ratio of the first natural period of the structure with full reservoir & flexible foundation case to the empty reservoir & flexible foundation case. Similarly,  $R_f$  is the ratio of the first natural period of the structure with flexible foundation & empty reservoir case to the rigid foundation & empty reservoir case. The damping ratio was calculated as 10% from the above equation. Mass and stiffness proportional Rayleigh Damping which produced 10% effective damping ratio in the first mode of the structure was used in the analyses. The first four natural periods together with their mode shapes are presented in Figure 3-2.

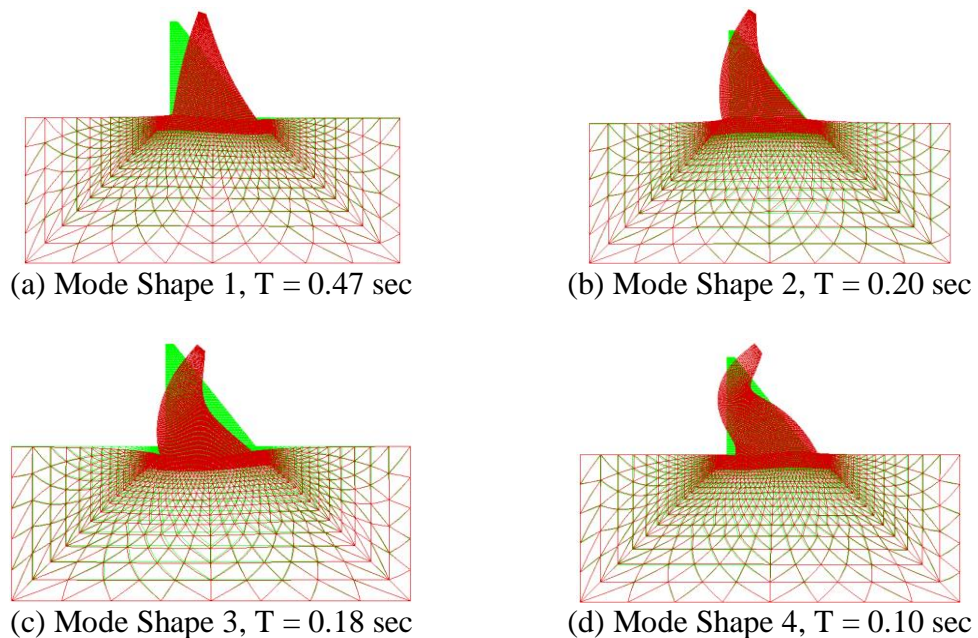


Figure 3-2 Mode Shapes

A constant time increment of 0.005 was used in the transient analyses. The convergence norm for both the residual displacement and force criteria was selected as 0.001. After the application of self-weight of the dam, hydrostatic load was applied and the dam model was subjected to several ground motions with different intensities.

### **3.2.1 Incremental Dynamic Analysis**

In incremental dynamic analysis (IDA), the structure is subjected to a set of ground motions which are scaled to multiple levels of intensity so that the relationship between the damage and intensity measures is obtained. The natural (unscaled) ground motions are scaled with a positive scaling factor that increases incrementally (Vamvatsikos and Cornell, 2002). The intensity measure (IM) is a positive scalar that depends on the intensity of a ground motion and increases incrementally with the scaling factor. Some common examples of IMs for the design or evaluation of buildings are the peak ground acceleration (PGA), peak ground velocity (PGV) and the 5% damped spectral acceleration at the structure's first-mode period ( $S_a(T_1, 5\%)$ ) (Vamvatsikos and Cornell, 2002).

The damage measure (DM) is a positive observable scalar, which can be found from the output of the non-linear dynamic analysis results. The quantification can be subjective based on the user's goals (design or evaluation) and constraints (capability of the analyses tools and time constraints). Some common response parameters used are the maximum base shear or maximum crest displacement of a structure, which are sometimes used as damage measures for ductile structures. However, the use of these parameters as damage measures includes the intrinsic assumption of elastic-perfectly plastic behavior, such as the perceived behavior in well-reinforced ductile buildings. The behavior of a dam monolith is different from such a well-defined response, as such, a seismic demand parameter, such as the crest displacement, can hardly be termed as a damage measure for this monolith. A more practical damage

measure, in terms of total cracking of the monolith, is investigated in this section along with the usual seismic demand parameters presented above.

### **3.3 Selection of Ground Motions**

In order to perform IDA of the 80 m high concrete gravity dam monolith, a set of 21 ground motions were selected (Table 3-1) so that the effect of different characteristics of ground motions could be investigated with the effect of different scaled levels. The motions were selected from Pacific Earthquake Engineering Research (PEER) strong motion database which were recorded on rock or stiff soil (type A or B of USGS) that had large magnitudes ranging from 6 to 7.6 and epicentral distances of 2 to 39 km, in accordance with FEMA440. To perform IDA, selected ground motions were scaled such that the spectral acceleration at the dam's first natural period (0.47 sec) was scaled from 0.4g to 0.8g with 0.05g increments. The spectral accelerations of these ground motions are presented in Figure 3-3. These target levels led to the use of scale factors ranging from 0.22 to 6.68.

Table 3-1 Selected Ground Motions

No	Earthquake Name	Component	Moment Magnitude	PGA (g)	PGV (cm/s)	R (km)	USGS Soil Type	Sa(5%) at T <sub>1</sub> (g)
1	Imperial Valley, 1979	315 degree	6.5	0.204	16.1	14.2	B	0.307
2	San Fernando, 1971	90 degree	6.6	0.110	13.3	31.7	B	0.318
3	San Fernando, 1971	270 degree	6.6	0.136	5.6	38.9	B	0.120
4	Landers, 1992	0 degree	7.3	0.171	20.2	23.2	B	0.290
5	Loma Prieta, 1989	0 degree	6.9	0.512	41.2	13.0	B	0.543
6	Loma Prieta, 1989	67 degree	6.9	0.357	28.6	11.6	B	0.842
7	Loma Prieta, 1989	270 degree	6.9	0.244	20.3	21.4	B	0.720
8	Morgan Hill, 1984	90 degree	6.2	0.292	36.7	11.8	B	0.484
9	Northridge, 1994	360 degree	6.7	0.514	52.2	22.6	B	1.153
10	Düzce, 1061 Lamont	E	7.1	0.134	13.7	15.6	B	0.246
11	Manjil, Abbar - ABBAR	Longitudinal	7.37	0.515	43.8	12.6	B	0.703
12	Tabas	Transverse	7.35	0.852	98.2	2.1	A	1.860
13	Loma Prieta, Gilroy	337 degree	6.9	0.325	22.3	11.6	B	0.566
14	Northridge, Burbank – Hw Rd.	330 degree	6.7	0.163	8.5	20	B	0.275
15	Northridge, 24088 Pacoima	360 degree	6.7	0.433	51.5	8.2	B	1.091
16	Spitak	0 degree	6.8	0.199	28.6	30	B	0.391
17	Cape Mendocino 1992	0 degree	7.1	1.497	127.4	8.5	A	1.582
18	Chi-Chi, Taiwan, 1999	E	7.6	0.133	39.8	14.3	A	0.196
19	Kocaeli – Gebze, 1999	0 degree	7.4	0.244	50.3	17	A	0.431
20	Kocaeli – İzmit, 1999	90 degree	7.4	0.22	29.8	4.8	A	0.341
21	Palm Springs, 1986	270 degree	6.0	0.612	31.5	7.3	A	0.922

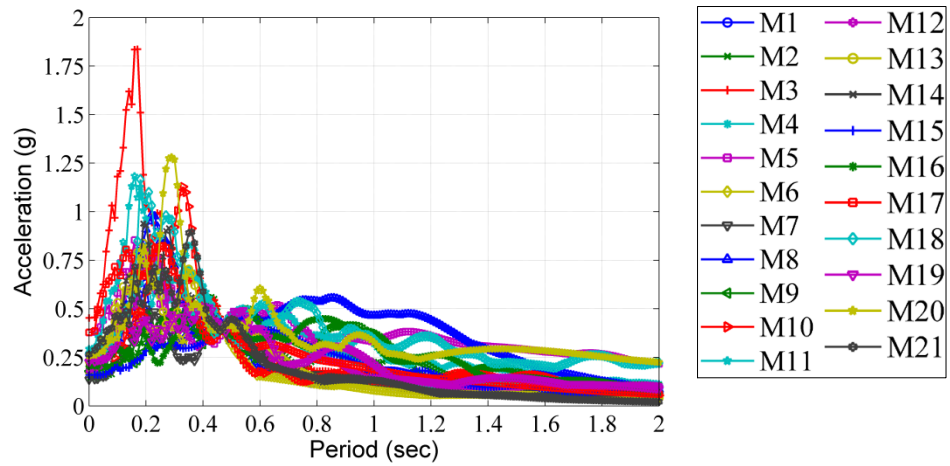


Figure 3-3 Acceleration Response Spectra (Scaled at  $T_1$ ) for the Selected Ground Motions

### 3.4 Results of IDA

A total number of 189 nonlinear transient analyses were conducted for the IDA. The cracking (both open and closed) at the end of the time history for all scales of different ground motions are presented in Figure 3-4. It can be seen from this figure that, the cracking initiates from the base of the dam at the upstream face. Later, a partial crack occurs at the base of the dam at the downstream face and as a general trend, cracking at the dam body first initiates from the downstream face. When the intensity of the motion increases, downstream cracks join the upstream cracks.

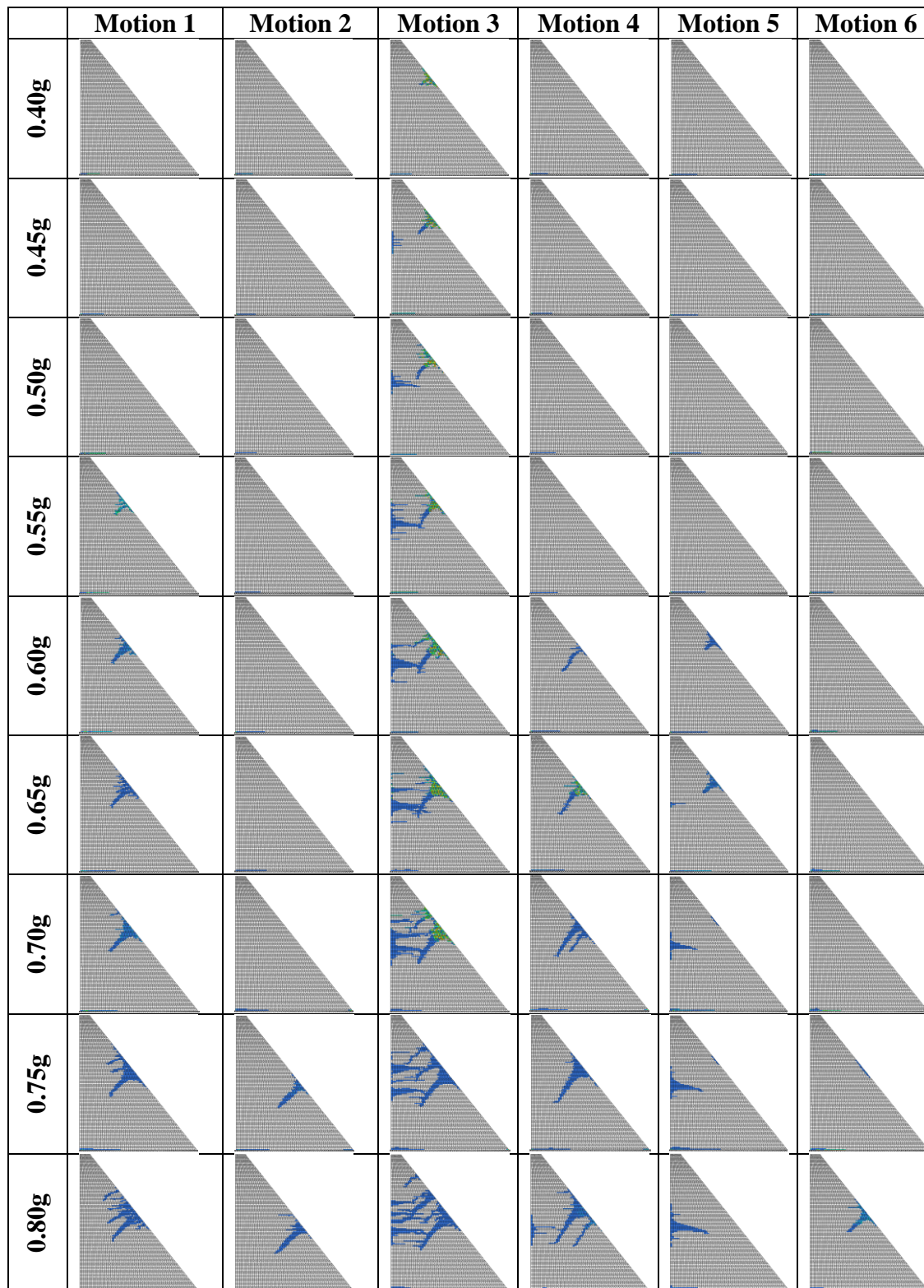


Figure 3-4 Cracking Schemes from the IDA

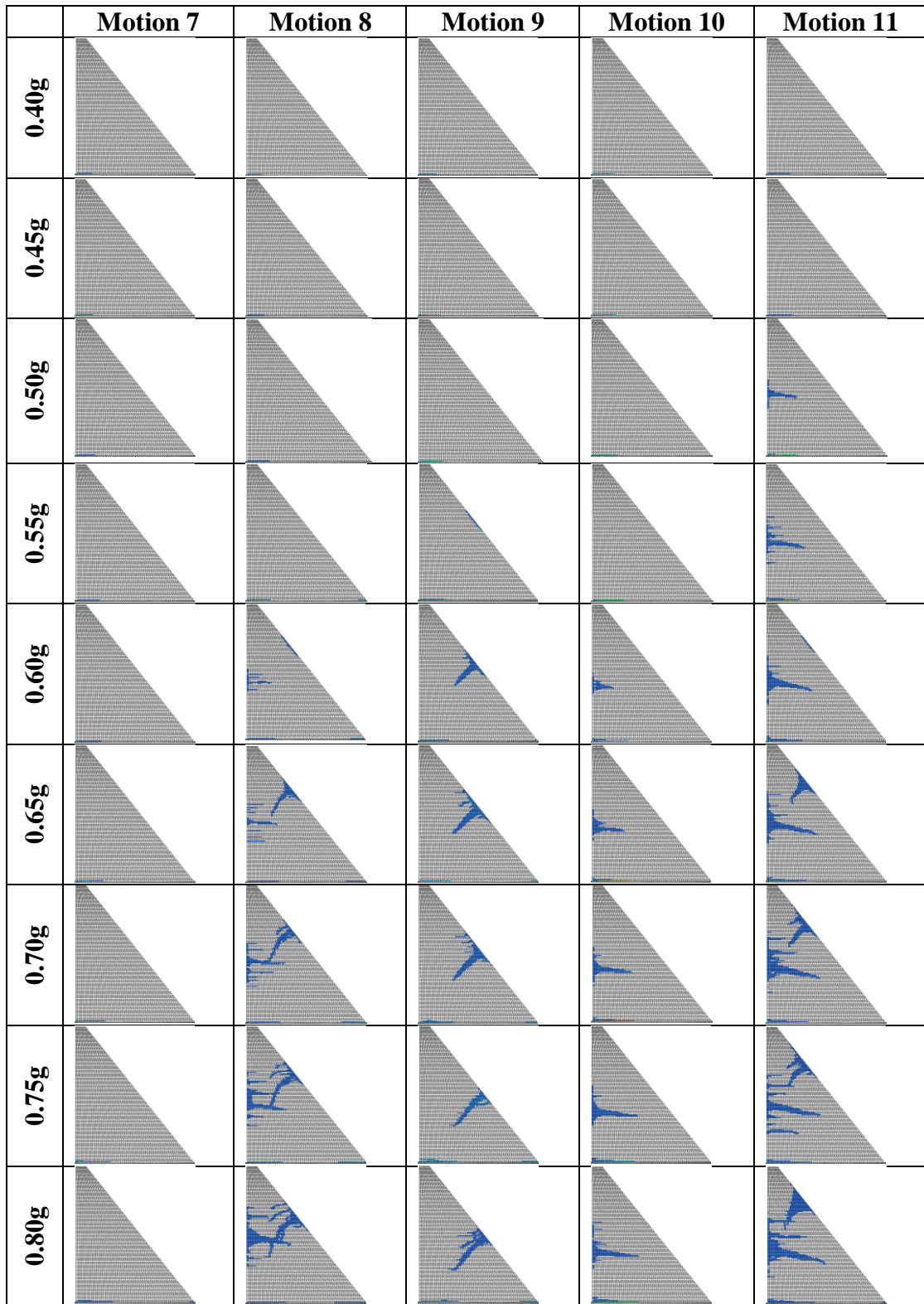


Figure 3-4 (Continued) Cracking Schemes from the IDA

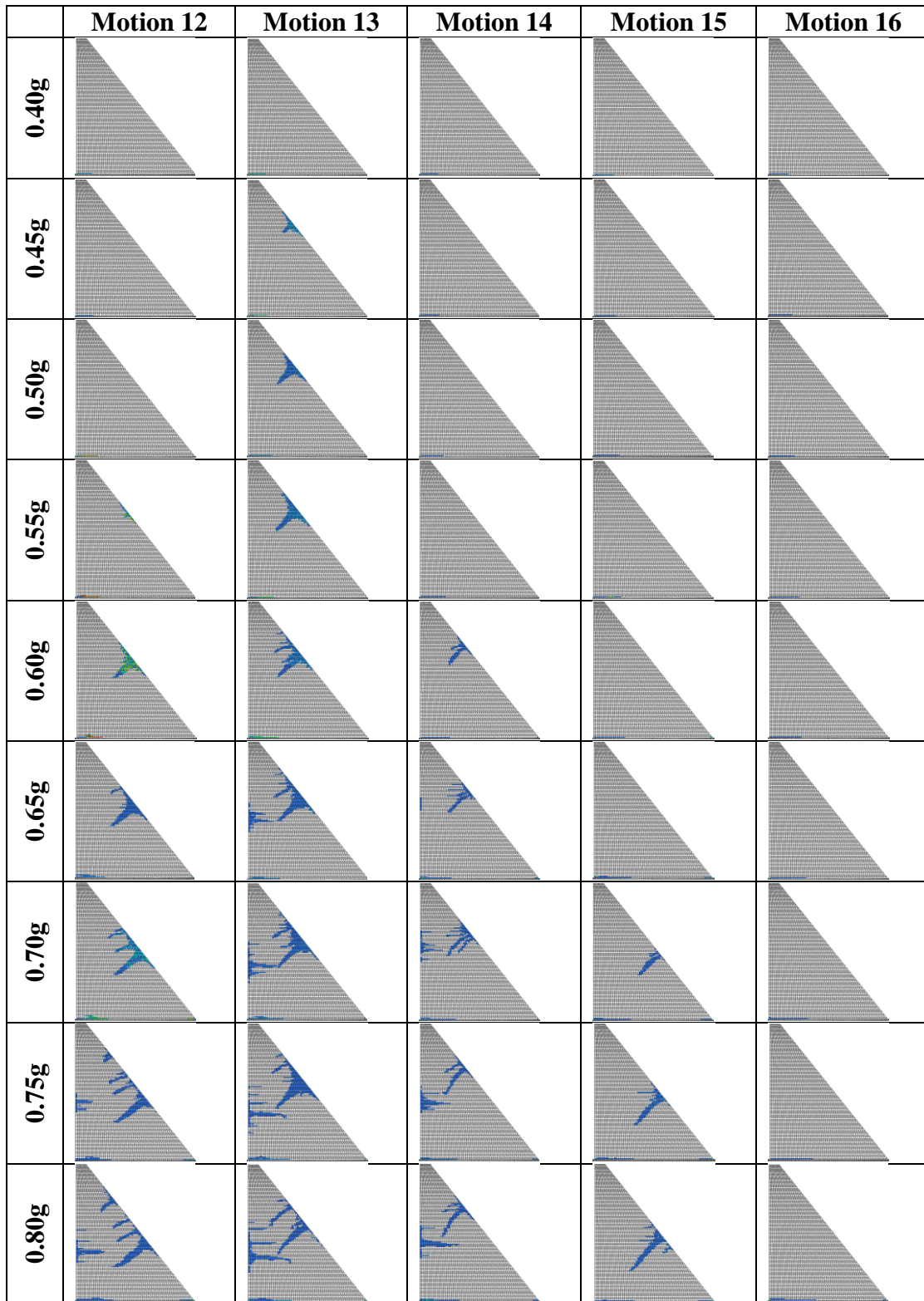


Figure 3-4 (Continued) Cracking Schemes from the IDA

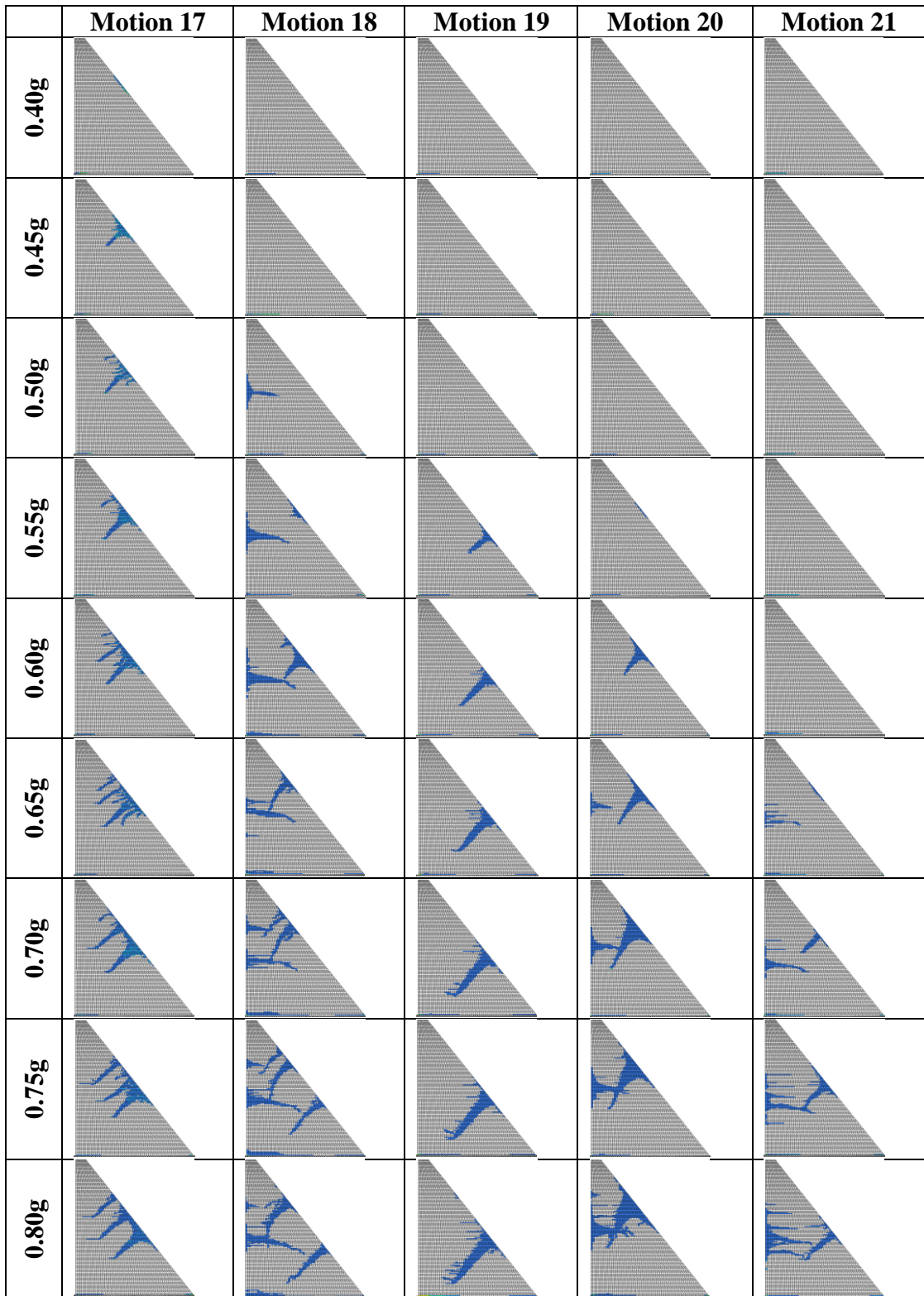
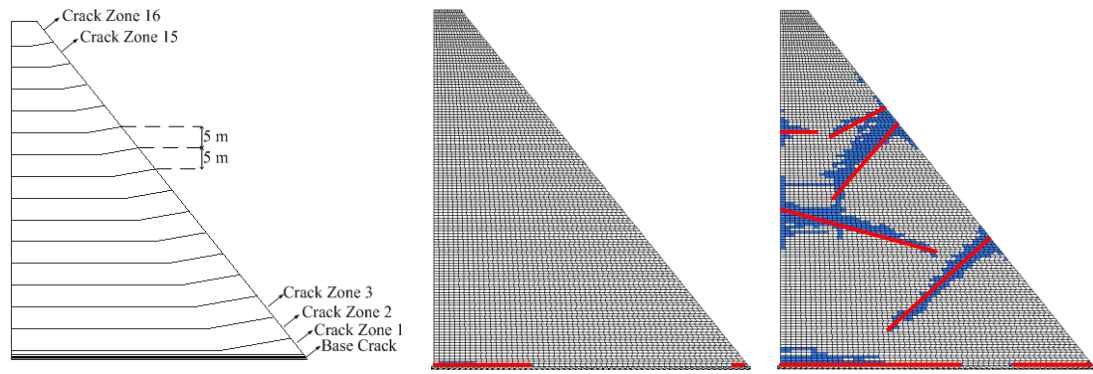


Figure 3-4 (Continued) Cracking Schemes from the IDA

The selection of a damage measure for a gravity dam monolith, similar to the use of a parameter like story drift ratio in buildings, is a significant challenge. First of all, field or experimental data on dams that has undergone significant damage is extremely scarce. Secondly, a numerical index should to be tied to some qualitative performance level which is still subjective. Performance levels are still widely debated within the dam engineering community. Therefore, a relatively simpler choice is made in this study and the total crack length within the dam body was chosen as the damage measure (Kanenawa et al., 2004). Cracks may start at various heights on the dam body, and propagating perpendicular to the upstream (horizontal cracks) and the downstream (inclined cracks) face. Accordingly, the dam body is divided into 17 crack initiation zones with 5 m increments, the first one corresponding to the cracking that would occur at the base, and the sequential ones corresponding to cracks that will form in these zones within the height of the increment (Figure 3-5). In accordance with El-Aidi and Hall (1989), if more than one crack occurred in one of the crack zones, the longest crack was taken into account and the other cracks were neglected due to the well-known smearing of damage to the nearby elements along the main crack in the constitutive model. Some minor cracks in the upstream direction (that did not propagate towards the downstream cracks) were also neglected. As a demonstration of the process, the individual cracks taken into account for motion 18, scaled to 0.80g are presented in Figure 3-5 with red lines. The total crack length was calculated as 174 m for this example; 117 m in the upstream direction and 57 m in the downstream direction.



(a) A schematic drawing of the crack zones  
 (b) Mildly-damaged cracked scheme (motion 7,  $S_a$  scaled to 0.80g)  
 (c) Severely-damaged cracked scheme (motion 18,  $S_a$  scaled to 0.80g)

Figure 3-5 Crack Zones and Cracking Schemes

The effect of damage on the structure in terms of extending the fundamental period was also recognized and the elongated natural period and its effect were investigated. By simulating the discontinuities, with decreasing the moduli of the cracked elements, in the upstream and downstream sides separately in Eigen analyses, the change in the fundamental period was compiled, for each motion, as given in Figure 3-6. The obtained range was an upper bound on the damaged period considering the facts that not every crack is open during a cycle of motion and the cracks open and close (upstream and downstream side usually alternating) during a given earthquake shaking. When the elongated period due to the upstream and downstream cracking was investigated separately, it was observed that the influence of the upstream cracking on the period elongation was very significant, unlike the downstream cracking. With the increase in the length and number of upstream cracks, the period of the dam elongates considerably, by as much as 3 times of the initial period (motion 18, scaled to 0.80g). The effect of downstream cracking was significantly less; the elongation was limited to 20%.

At average, the period was determined to increase by 45% due to the damage

occurring on the system, an increase of natural period from 0.47 sec to 0.68 sec. Even if the damaging effect of motion 18 is disregarded, the period increase is 42%. A second degree polynomial can be fitted to the mean of the estimates for each design level with a correlation coefficient of 0.68 (shown in magenta in Figure 3-6); however, the correlation coefficient was increased to 0.81 when motion 18 is disregarded.

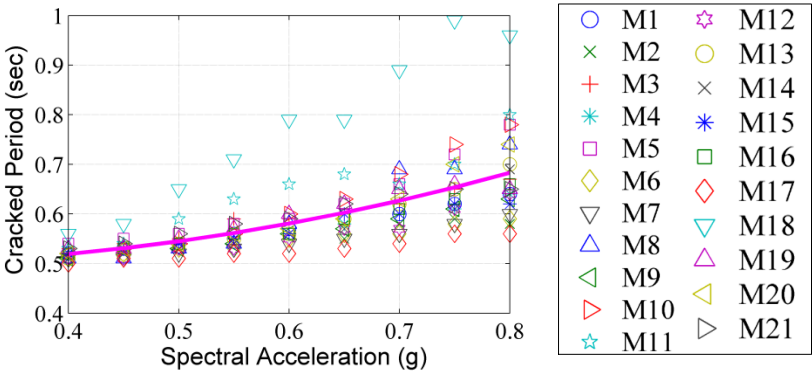


Figure 3-6 First Cracked Period of the Dam

For the design of such dams or large infrastructure projects, seismic hazard analyses are commonly conducted with the purpose of obtaining a target design spectrum that is utilized for generation of ground motions. Hence, spectral acceleration is most of the time the sole IM used in the design of such structures. In this study, apart from the spectral values  $S_a$ , the peak ground velocity (PGV) and spectral velocity  $S_v(T_1, 5\%)$  was also considered. In Figure 3-7, the variation of damage on this typical monolith with different damage measures are presented together with their correlation coefficients ( $R^2$ ), namely different spectral acceleration levels (i.e. different targets), peak ground acceleration (PGA), spectral velocity at first natural period ( $S_v$ ), peak ground velocity (PGV), arias intensity and specific energy density. The spectral velocity as a prediction parameter yielded the highest  $R^2=0.81$  value compared to other intensity measures. However, even for this parameter, there is a noticeably wide spread of the data points (subjectively) around the best fit. Spectral acceleration, the traditional parameter used in the design and evaluation of structures, did a very poor job in predicting the damage occurring on the dam monolith. Given

the poor performance of these commonly used parameters, prediction using a more involved formula using different IM values was investigated.

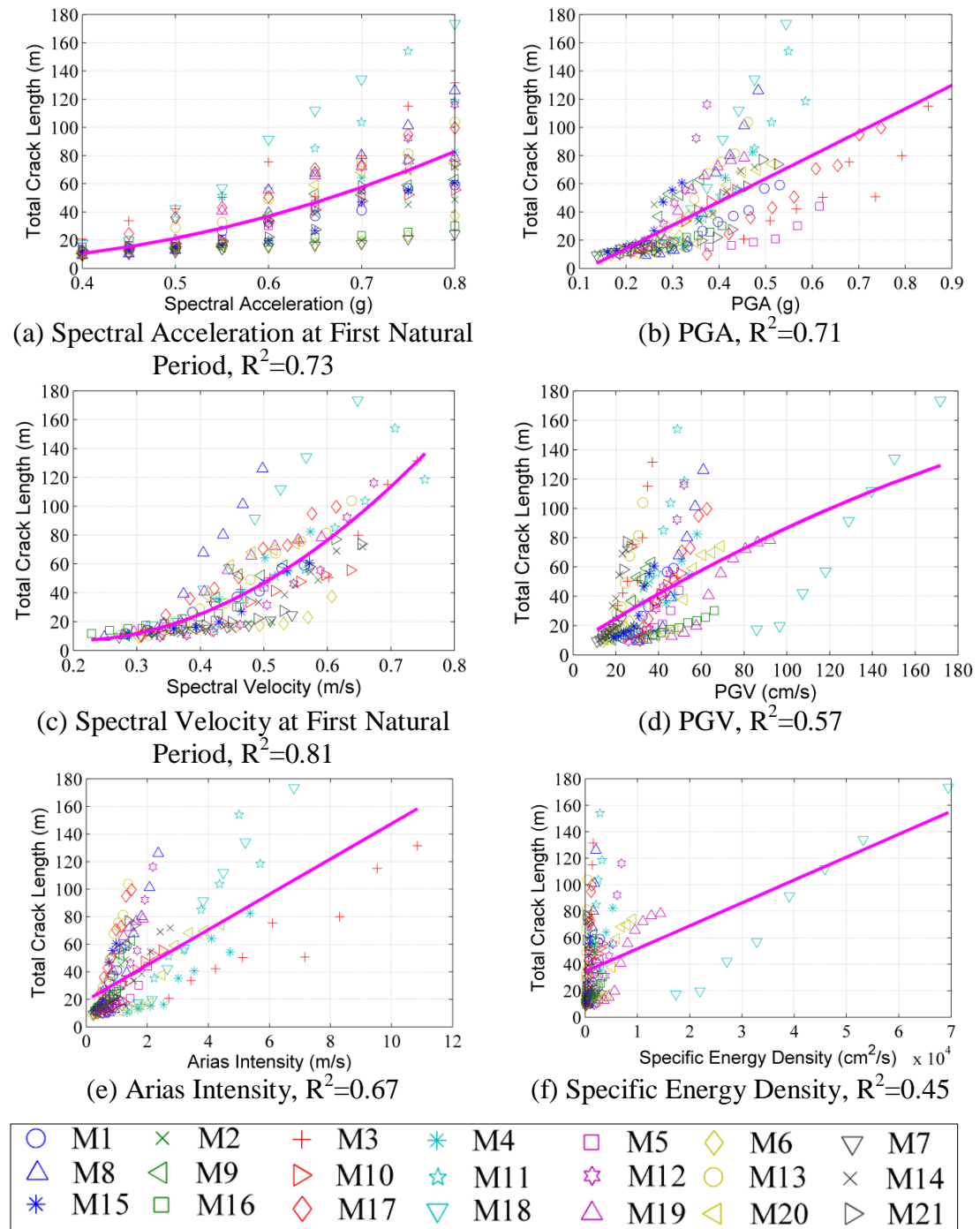


Figure 3-7 Total Crack Length of the Dam vs. Different Intensity Measures

A preliminary relationship between the total crack length and the considered intensity measures, PGV and  $S_v(T_1,5\%)$ , is proposed in Equation 3-2. The predictions on the crack length obtained using the proposed formulation is compared to the analyses results in Figure 3-8. In this equation (3-2), PGV represents the peak ground velocity of the motion and  $S_v(T_1,5\%)$  represent the spectral velocity at the structure's first natural period. From Figure 3-8, it can be observed that the chosen measure successfully correlates with the behavior of the dam, with a correlation coefficient of 0.90. When the IM is above 0.45, it can be seen that the total crack length increases rapidly (Figure 3-8); therefore, it is suggested that in design, the IM should be kept below 0.45.

$$IM = 1 - \left| \log(PGV) \times \log(S_v(T_1, 5\%)) \right| - \log(S_v(T_1, 5\%)) \tag{3-2}$$

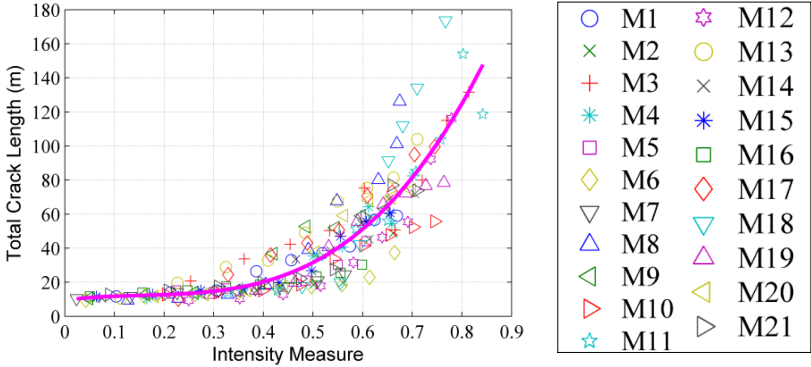


Figure 3-8 Total Crack Length of the Dam with the Proposed Intensity Measure

Overall, in lieu of the spectral acceleration quantity that is extensively used in earthquake engineering, the velocity characteristics of the ground motion and the spectral velocity appear to be the significant factors that affect the damage occurring on the system. With the consideration of the velocity characteristics of the ground motion, it was possible to estimate a bound on the damage level on the monolith for the chosen target level. A similar estimation of damage on the system using spectral acceleration of the motion can be widely off the mark, as shown in Figure 3-7. This issue presents a significant problem with the current methodology of assessing seismic hazard for such structures, which is conducted in terms of defining a target response spectrum. The crack propagation on the monolith composed of the brittle

concrete material was determined to be very much dependent on the velocity characteristics of the ground motion indicating that the duration spent at certain force levels are as important as the force levels.

Following the tradition of decades of spectrum use along with the much accepted procedure of reduction for ductility, a general understanding is accepted to govern the performance of buildings: some damage is expected for a given target level with a significant reduction ( $1/8^{\text{th}}$  to  $1/4^{\text{th}}$ ) of the design force level. However for a very rigid, massive structure like a dam monolith comprised of the brittle material concrete, the spectral level governs only the level in which initial cracking will occur: the duration and velocity characteristics of the motion is much more important in the final performance of the given section. Therefore the use of spectral levels is correct only for designs within the elastic range: much more information about the earthquake time history is required in order to design or evaluate the same structure in the nonlinear range.

In order to quantify the uncertainty in the velocity and duration characteristics of the ground motion, the use of many motions and scaling factors such as suggested in FEMA440 appears to be a reasonable option, given that provision of target ground velocity or duration information for seismic hazard at a local site is still quite far away. The use of the variability in recorded motions to address the variability in the velocity and duration for a target level motion at a site is more feasible at this stage, as this method typically requires the use of more than 10 motions in the analyses. Use of a very few (typically 3) spectrum fitted motions, in this sense, is not adequate for the determination of the level of performance of a system given the large variability in the performance level for different motions.

### **3.5 Pushover Analysis**

A pushover analysis (or nonlinear static procedure) can be defined as applying a static lateral force distribution on a given structure in order to estimate the seismic

structural deformations (FEMA, 1997). It is a widely used method to determine the performance limits of structures. Pushover analyses for buildings are widely popular given the relative ease of use of the methodology along with the well-defined performance limits generally obtained from similar analyses.

Given the significant cost of IDA analyses, the pushover analysis is an attractive tool also for dam monoliths in order to understand the behavior better using a much faster analyses approach. However, there are two significant problems in applying such analyses to monoliths: First of all, some component of the lateral force on a dam system (i.e. hydrodynamic force) is frequency dependent, therefore it is very hard to ascertain the shape of the hydrodynamic force on a dam monolith given that it depends on the nature of the ground motion as well as structural properties. On the other hand, the lateral force on the structure, which is typically applied proportional to the first mode shape on such a structure is hardly reflective of the distribution of the force in later stages of a damaging motion. In other words, it is very hard to reflect a realistic force distribution on such a structure given the complexity of the damaged system unlike frame systems.

Given the complexities of applying pushover analysis technique to a dam monolith, the analysis given here was conducted with some basic assumptions simplifying the problem. The lateral load distribution was assumed as given in Equation 3-3a (Alembagheri and Ghaemian, 2012).

$$P(y) = F(y) + H(y) \quad (3-3a)$$

where  $P(y)$  is the total lateral load distribution that accounts for the contributions coming from the inertial effects,  $F(y)$  and hydrodynamic effects,  $H(y)$ .  $y$  is the height measured from the base of the dam. The hydrodynamic force distribution is derived from the Westergaard's added mass approach assuming incompressible reservoir fluid.  $F(y)$  and  $H(y)$  are defined in Equations 3-3b and 3-3c, respectively.

$$F(y) = \alpha \times b(y) \times \psi_1(y) \times \rho_c \quad (3-3b)$$

$$H(y) = \frac{7}{8} \rho_w \sqrt{h(h-y)} \quad \text{for } y \leq h \quad (3-3c)$$

where  $\alpha$  is defined as the weight factor,  $b$  is the dam width,  $\psi_1$  is the normalized first-mode shape of the dam,  $\rho_c$  is the density of concrete,  $\rho_w$  is the water density and  $h$  is the reservoir height. The weight factor,  $\alpha$ , was taken as 4 so that the total inertial load be 3 times the hydrodynamic load (Alembagheri and Ghaemian, 2012). The lateral load distribution is presented in Figure 3-9.

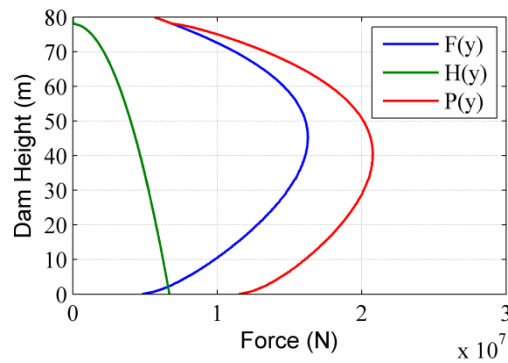


Figure 3-9 Total Lateral Load Distribution for the Pushover Analysis

Pushover analyses were conducted for a full reservoir and an empty reservoir case. Also, the analyses were conducted with the load application into the downstream (referred to as direction 1) and the upstream faces (referred to as direction 2) of the dam. A schematic drawing of the loading directions is presented in Figure 3-10.

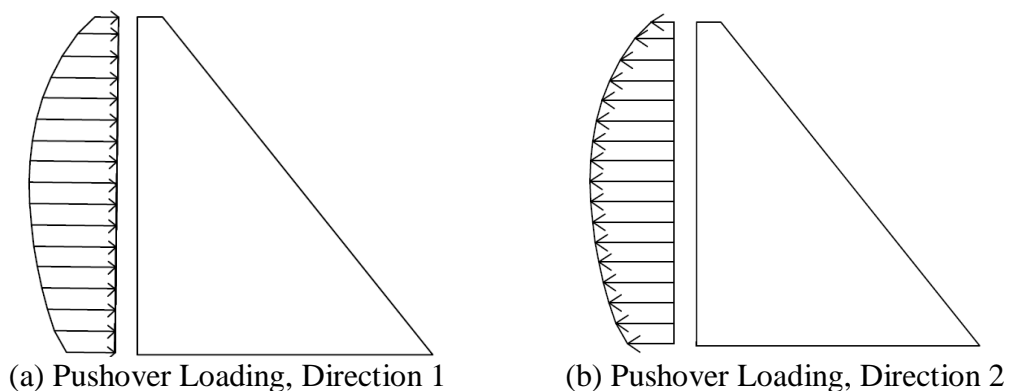


Figure 3-10 A Schematic Drawing of the Pushover Loading Directions

The cracking schemes obtained using these simple load distributions are shown in Figure 3-11.

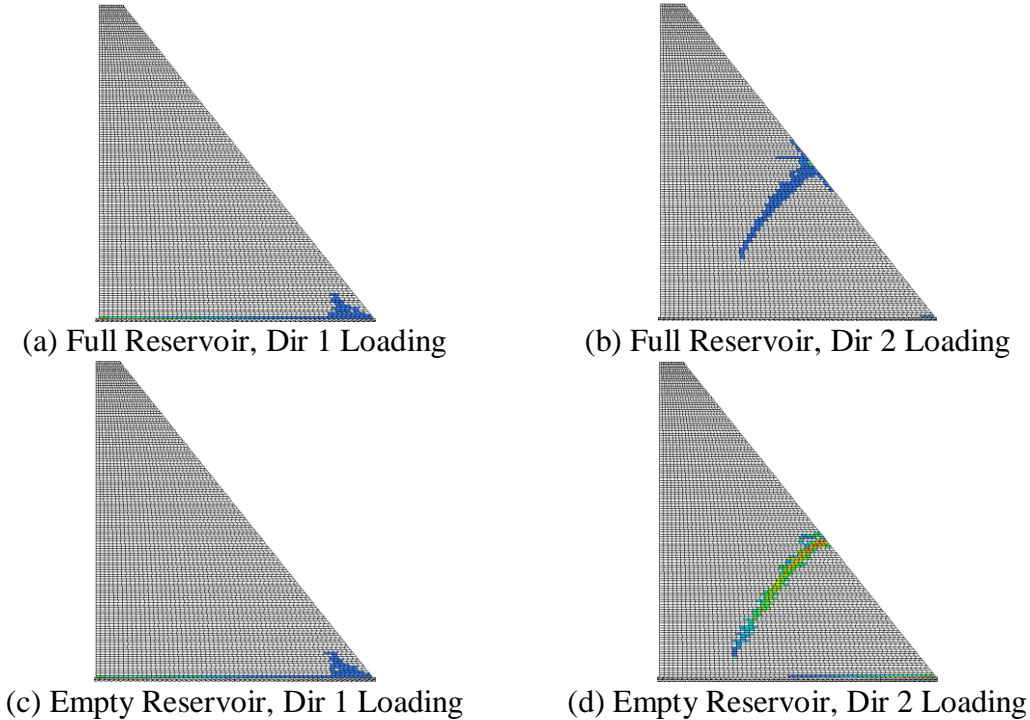


Figure 3-11 Cracking Scheme of the Pushover Analyses

As given in Figure 3-11, the pushover analyses resulted in significantly different cracking distribution on the dam compared to the IDA analyses results. For the full and empty reservoir cases, the upstream-downstream direction loading damaged the base of the dam completely: the system failed when the crack starting at the upstream face reached the downstream face. For the other direction loading, the crack occurred parallel to the downstream face propagating towards the base for the full reservoir case. Without the reservoir, this crack was coupled by a crack forming at the base on the downstream side.

Notably, the distribution of cracking from the pushover analyses was much different from the IDA analyses, much more concentrated on the base of the dam. None of the IDA analyses showed a base crack traversing between the upstream and downstream

face, or even the monolith base having a crack traversing more than 50% of its length. The load distribution in a given time history analysis was obviously much more different than the one assumed in pushover analyses as the failure behavior was distinctly different for these two methods. The total crack length for full reservoir and empty reservoir case was obtained as 104 m and 145 m, respectively, compared to the maximum crack length obtained from IDA analyses, which was 174 m. The results are reasonable only if the damage measure specified at crack length at face value. Although the total crack length could be said to be estimated close to the IDA results for the empty reservoir case, the resulting cracking scheme does not match with IDA. In the IDA analyses, due to redistribution of the loading, the cracking was spread over the dam height; however, in the pushover analysis such a redistribution could not be obtained.

The base shear versus the crest displacement for the full reservoir case is compared for IDA and pushover analysis for both loading directions in Figure 3-12. The mean base shear obtained for all the motions at a given displacement is presented. The pushover curve and the IDA curve were very similar in the initial, elastic part. On the other hand, the curves started to diverge from each other around 10 cm of crest displacement. Base shear values obtained from the transient analyses were as high as 50% from the pushover analyses, clearly showing the different load carrying pattern for both analyses. Pushover analyses significantly underestimated the base shear as well as lateral displacement capacity of the dam for direction 2 as well.

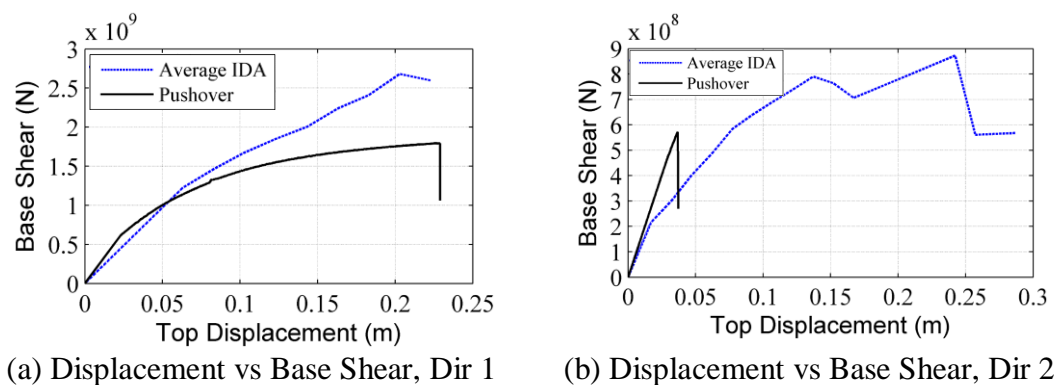


Figure 3-12 IDA vs. Pushover Analyses Results

Given the significant difference between the results of the IDA and pushover analyses, it is quite evident that the pushover analysis methodology should be significantly changed for its proper application to dam monoliths. The distribution of loading is a significant issue both for determining the hydrodynamic contribution as well as reflecting the change of the inertial force to the system. From the IDA analyses, it was observed very clearly that once the base of the dam cracks to some extent at the upstream and downstream faces, the crack initiation is directly transferred to points higher up on the dam body. For the remaining time of the motion, the majority of the cracks occur further away from the base and propagate towards inside the dam body. An adaptive methodology reflecting the effect of damage on the load distribution on the dam body is required in order to obtain a more realistic damage distribution similar to the IDA analyses results.

## CHAPTER 4

### CONCLUSION AND FUTURE PLANS

#### 4.1 Conclusion

In this study, the behavior of a concrete gravity dam monolith was investigated using the incremental dynamic analysis (IDA) to determine the development of damage on the monolith and the corresponding cracking patterns.

First, the constitutive model was calibrated to the experimental data so that the ability of the model to simulate the fracture in this material was verified. The following conclusions were drawn based on the results of the simulations.

- ❖ The shape of the post-peak curve and the strength determine the crack propagation process. For all the three tests, it was observed that softening functions with faster declining curves after the peak were more appropriate for use, such as Hordyk or exponential models.
- ❖ For the finer meshes approaching the limits of macro-modeling of concrete, concentration of the stresses led to significant stress demands, and required the assumption of higher tensile strength values in order to reproduce test behavior. However, within current limitations of computational power, modeling of monoliths is still well within macro modeling limits. The 1.5x dynamic strength, as prescribed by USACE (1995) appears appropriate for dynamic modeling of concrete monoliths.
- ❖ Both rotating and fixed crack models yielded similar cracking patterns predicting the crack propagation correctly for the experiments. However, the displacement predictions were rather off the mark. Further study in

constitutive modeling is required to reproduce accurate displacement of cracked concrete models.

- ❖ Shear retention factor and the damping behavior within the crack appear to be important factors in the determination of correct crack mouth displacements. However, these are very complex issues significantly related to aggregate interlocking, crushing within the crack, and possibly the number of cycles the cracks go through. Further testing is required in order to address these issues with a more complicated constitutive model.

Next, IDA was performed on an 80 m high concrete gravity dam monolith. The following conclusions were drawn based on the results from this study.

- ❖ The damage development on the monolith is significantly affected by the velocity characteristics of the ground motion and the spectral velocity, in lieu of the spectral acceleration values commonly used in the design of these structures. The spectral quantities such as PGV and  $S_v(T_1, 5\%)$ , affected the cracking behavior of dam significantly.
- ❖ Upstream cracks change the behavior of the monolith much more comprehensively compared to the inclined downstream cracks. The natural period increased to as high as 3 times the initial period with upstream cracking compared to a maximum increase of 1.2 times for the downstream cracking. An intensity measure based on PGV and  $S_v(T_1, 5\%)$  was proposed for the estimation of the damage level of the monolith.
- ❖ The use of spectral acceleration to prescribe hazard on a site is only satisfactory if the design/evaluation of the dam structure is carried out in the linear range. Spectral acceleration only defines the initiation of cracking for a particular system: very different performance may be observed for a system for three motions with identical spectral acceleration response, such as motions fitted to the same target spectrum. Use of three motions for determination of nonlinear performance could be highly off the mark.
- ❖ In order to quantify the uncertainty in the velocity and duration characteristics of the ground motion (defining the damage on the system), the use of the methodology as suggested in FEMA440 appears to be a reasonable option.

The use of the variability in recorded motions to address the variability in the velocity and duration for a target level motion at a site is more feasible given that seismic hazard at a site could hardly be presented in the form of velocity and duration response at this stage.

Finally, the results of the IDA were compared to the static pushover analysis results in order to evaluate the scope of possible use of such analyses for determining the performance levels of dams. The pushover analysis with a simple loading methodology was not able to correctly represent the damage and the load redistribution on the system as seen in the dynamic analyses, underestimating the cracking scheme and base shear. Significantly more effort has to be made in developing an adaptive loading scheme for the pushover methodology to be applicable to similar systems.

## **4.2 Future Plans**

Some avenues of future study based on the findings in this study are given below.

- ❖ In order to successfully simulate the more complex behavior of dams, a new constitutive model for accurately representing the concrete behavior is required. This model needs to incorporate a transient damping with respect to the state of a crack as well as the incremental loss of shear retention in a crack with respect to the number of opening-closing cycles the crack undergoes.
- ❖ The effect of the vertical component of a ground motion was not considered in the IDA analyses. The effect of the vertical component and the interaction between the two-directions of ground motion will be considered in a future study.

- ❖ The proposed intensity measure was obtained for a selected dam geometry. The measure can be generalized by taking the dimensions of the dam (upstream, downstream slopes and the height) into account.
- ❖ A pushover method to more successfully predict the behavior of dams needs to be developed. The redistribution of inertial and hydrodynamic loading should be represented in a staged load application based on the damage state in this procedure.

## REFERENCES

- Aldemir, A., Binici, B., Canbay, E., Kurç, Ö., & Arıcı, Y. (2013). Seismic Performance Evaluation of a Concrete Gravity Dam by Using Pseudo Dynamic Testing. *The 2013 World Congress on Advances in Structural Engineering and Mechanics*, Jeju.
- Alembagheri, M., & Ghaemian, M. (2012). Seismic Assessment of Concrete Gravity Dams Using Capacity Estimation and Damage Indexes. *Earthquake Engineering and Structural Dynamics*, Vol. 42, pp. 123-144.
- Ali, M. H., Alam, M. R., Haque, M. N., & Alam, M. J. (2012). Comparison of Design and Analysis of Concrete Gravity Dam. *Natural Resources*, Vol. 3, pp. 18-28.
- Araujo, J. M., & Awruch, A. M. (1998). Probabilistic Finite Element Analysis of Concrete Gravity Dams. *Advances in Engineering Software*, Vol. 29, pp. 97-104.
- Asteris, P. G., & Tzamtzis, A. D. (2003). Nonlinear Seismic Response Analysis of Realistic Gravity Dam-Reservoir Systems. *International Journal of Nonlinear Sciences and Numerical Simulation*, Vol. 4, pp. 329-338.
- Basu, U., & Chopra, A. K. (2003). Perfectly Matched Layers for Time-Harmonic Elastodynamics of Unbounded Domains: Theory and Finite-Element Implementation. *Computer Methods in Applied Mechanics and Engineering*, Vol. 192, pp. 1337-1375.
- Bhattacharjee, S. S., & Leger, P. (1994). Application of NLFM Models to Predict Cracking in Concrete Gravity Dams. *Journal of Structural Engineering*, Vol. 120, pp. 1255-1271.
- Bazant, Z. (1986). Mechanics of Distributed Cracking. *Applied Mechanics Reviews*, Vol. 39, pp. 675-705.
- Binici, B., Arıcı, Y., Kurç, Ö., Canbay, E., Aldemir, A., & Soysal, B. F. (2012). *TÜBİTAK Araştırma Projesi Gelişme Raporu*. Ankara.
- Carpinteri, A., Valente, S.V., Ferrara, G., & Imperato, L. (1992). Experimental and Numerical Fracture Modelling of a Gravity Dam. *Fracture Mechanics of Concrete Structures*, pp. 351-360.
- Chopra, A. K. (2004). Estimating Seismic Demands for Performance-Based Engineering of Buildings. *The 13th World Conference on Earthquake Engineering*, Vancouver.

Chopra, A. K. *Dynamics of Structures Theory and Applications to Earthquake Engineering, 3rd Ed.*, Pearson Prentice Hall, New Jersey, 2007.

Chopra, A. K., & Gupta, S. (1981). Hydrodynamic and Foundation Interaction Effects in Earthquake Response of a Concrete Gravity Dam. *Journal of Structural Division, ASCE, Vol. 107*, pp. 1399-1412.

Chuhan, Z., Jianwen, P., & Jinting W. (2009). Influence of Seismic Input Mechanisms and Radiation Damping on Arch Dam Response. *Soil Dynamics and Earthquake Engineering, Vol. 29*, pp. 1282-1293.

Çalayır, Y., & Karaton, M. (2005). Seismic Fracture Analysis of Concrete Gravity Dams Including Dam-Reservoir Interaction. *Computers and Structures, Vol. 83*, pp. 1595-1606.

de Borst, R., Remmers, J. J. C., Needleman, A., & Abellan, M. A. (2004). Discrete vs Smeared Crack Models for Concrete Fracture: Bridging the Gap. *International Journal for Numerical and Analytical Methods in Geomechanics, Vol. 28*, pp. 583-607.

Devlet Su İşleri Genel Müdürlüğü, <http://www.dsi.gov.tr/>, last visited on December 2013.

El-Aidi, B., & Hall, J. F. (1989). Non-linear Earthquake Response of Concrete Gravity Dams. Part 2: Behavior. *Earthquake Engineering and Structural Dynamics, Vol. 18*, pp. 853-865.

Fajfar, P. (2000). A Nonlinear Analysis Method for Performance-Based Seismic Design. *Earthquake Spectra, Vol. 16*, pp. 573-592.

FEMA. (2005). *Improvement of Nonlinear Static Seismic Analysis Procedures*. FEMA 440: Washington, D. C.

FEMA. (1997). *NEHRP Guidelines for the Seismic Rehabilitation of Buildings*. FEMA 273: Washington, D. C.

Fenves, G., & Chopra, A. K. (1985). Effects of Reservoir Bottom Absorption and Dam-Water-Foundation Rock Interaction on Frequency Response Functions for Concrete Gravity Dams. *Earthquake Engineering and Structural Dynamics, Vol. 13*, pp. 13-31.

Freeman, S. A., Nicoletti, J. P., & Tyrell, J. V. (1975). Evaluations of Existing Buildings for Seismic Risk – A Case Study of Puget Sound Naval Shipyard, Washington. *Proceedings of the U.S. National Conference on Earthquake Engineers*, Berkeley.

Ghanaat, Y., & Chudgar, A. K. (2007). *Seismic Design and Evaluation of Concrete Dams-An Engineering Manual*.

Hall, J. F., & Chopra, A. K. (1980). *Dynamic Response of Embankment, Concrete Gravity and Arch Dams Including Hydrodynamic Interaction*. Earthquake Engineering Research Center, University of California, Berkeley, UCB/EERC-80/39.

Hall, J. F., & Chopra, A. K. (1982). Hydrodynamic Effects in the Dynamic Response of Concrete Gravity Dams. *Earthquake Engineering and Structural Dynamics, Vol. 10*, pp. 333-345.

Hall, J.F. (1988). The Dynamic and Earthquake Behavior of Concrete Dams: Review of Experimental Behavior and Observational Evidence. *Soil Dynamics and Earthquake Engineering, Vol. 7*, pp. 57-121.

Hasan, R., Xu, L., & Grierson, D. E. (2002). Push-over Analysis for Performance-Based Seismic Design. *Computers and Structures, Vol. 80*, pp. 2483-2493.

International Commission on Large Dams, [http://www.icold-cigb.org/GB/Dams/role\\_of\\_dams.asp](http://www.icold-cigb.org/GB/Dams/role_of_dams.asp), last visited on December 2013.

Jiang, S., & Du, C. (2012). Seismic Stability Analysis of Concrete Gravity Dams with Penetrated Cracks. *Water Science and Engineering, Vol. 5*, pp. 105-119.

Kanenawa, K., Sasaki, T., & Yamaguchi, Y. (2004). Effects of Fracture Material Properties on Crack Propagation of Concrete Gravity Dams During Large Earthquakes. *The 13th World Conference on Earthquake Engineering*, Vancouver.

Kimata, H., Fujita, Y., Niimi, K., Niyamoto, D., Nakayama, K., & Ushida, Y. (2008). Seismic Safety of Concrete Gravity Dams Based on Dynamic Crack Propagation Analysis During Large-Scale Earthquakes. *The 14th World Conference on Earthquake Engineering*, Beijing.

Leger, P., & Boughoufalah, M. (1989). Earthquake Input Mechanisms for Time-Domain Analysis of Dam-Foundation Systems. *Engineering Structures, Vol. 11*, pp. 37-46.

Li, Q., Zhang, F., Zhang, W., & Yang, L. (2002). Fracture and Tension Properties of Roller Compacted Concrete Cores in Uniaxial Tension. *Journal of Materials in Civil Engineering, Vol. 14*, pp. 366-373.

Mansouri, A., Neshaei, M. A. L., & Aghajany, R. (2011). Fracture Analysis of Concrete Gravity Dam Under Earthquake Induced Loads. *Journal of Applied Sciences and Environmental Management, Vol. 15*, pp. 317-325.

- Mirzabozorg, H., & Ghaemian, M. (2005). Non-linear Behavior of Mass Concrete in Three-Dimensional Problems Using a Smeared Crack Approach. *Earthquake Engineering and Structural Dynamics*, Vol. 34, pp. 247-269.
- National Research Council. *Earthquake Engineering for Concrete Dams: Design, Performance, and Research Needs*, National Academy Press, Washington D.C., 1990.
- Ngo D., & Scordelis A. C. (1967). Finite Element Analysis of Reinforced Concrete Beams. *Journal of ACI*, Vol. 64, pp. 152-163.
- Nuss, L. K., Matsumoto, N., & Hansen, K. D. (2012). Shaken, but not Stirred – Earthquake Performance of Concrete Dams. *32nd Annual USSD Conference*, New Orleans
- Pal, W. (1976). Seismic Cracking of Concrete Gravity Dam. *Journal of Structural Division*, Vol. 102, pp. 1827-1844.
- Pekau, O. A., & Zhu, X. (2006). Seismic Behavior of Cracked Gravity Dams. *Earthquake Engineering and Structural Dynamics*, Vol. 35, pp. 477-495.
- Rashid, Y. R. (1968). Analysis of Prestressed Concrete Pressure Vessels. *Nuclear Engineering and Design*, Vol. 7, pp. 334-344.
- Rots, J. G. *Computational Modeling of Concrete Fracture*. Delft University of Technology, Delft, 1988.
- Rots J. G., & de Borst, R. (1988). Analysis of Mixed-Mode Fracture in Concrete. *Journal of Engineering Mechanics*, Vol. 113, pp. 1739-1758.
- Tinawi, R., Leger, P., Leclerc, M., & Cipolla, G. (2000). Seismic Safety of Gravity Dams: From Shake Table Experiments to Numerical Analysis. *Journal of Structural Engineering*, Vol. 126, pp. 518-529.
- TNO DIANA. *User's Manual*, R. 9.4.3, 2010.
- US Army Corps of Engineers. (1995). *Seismic Design Provisions for Roller Compacted Concrete Dams*. Washington, D. C: Engineering and Design, EP 110-2-12.
- US Army Corps of Engineers. (2003). *Time-History Dynamic Analysis of Concrete Hydraulic Structures*. Washington, D. C: Engineering and Design, EM 1110-2-6051.
- Vamvatsikos, D., & Cornell, C. A. (2002) Incremental Dynamic Analysis. *Earthquake Engineering and Structural Dynamics*, Vol. 31, pp. 491-514.

Westergaard, H. M. (1933). Water Pressures on Dams during Earthquakes. *American Society of Civil Engineers, Vol. 98*, pp. 418-433.

Yamaguchi, Y., Sasaki, T., Iwashita, T., Sasaki, S., & Kurahashi, H. (n.d.). *Evaluation of Tensile Cracks in Concrete Gravity Dams by Shaking Table Tests and Non-linear FEM Analyses with Smeared Crack Model*.

Yanmaz, A. M., *Applied Water Resources Engineering, 3rd Ed.*, METU Press, Ankara, 2006.

Yılmaztürk, M., *Three Dimensional Dynamic Response of a Concrete Gravity Dam*, Middle East Technical University, Ankara, 2013.